EGG-TMI-7811

PATENT CLEARED

cy 1

EGG-TMI-7811

INFORMAL REPORT

Idaho National Engineering Laboratory

Managed by the U.S. Department of Energy

THERMAL INTERACTION OF CORE MELT DEBRIS WITH THE TMI-2 BAFFLE, CORE-FORMER, AND LOWER HEAD STRUCTURES

A. W. Cronenberg
E. L. Tolman

EG&G Idaho

Work performed under DOE Contract No. DE-AC07-76ID01570

EGG-TMI-7811

THERMAL INTERACTION OF CORE MELT DEBRIS WITH THE TMI-2 BAFFLE, CORE-FORMER, AND LOWER HEAD STRUCTURES

August W. Cronenberg[a]
E. L. Tolman

Published September 1987

EG&G Idaho, Inc.
Idaho Falls, Idaho 83415

Prepared for the
U.S. Department of Energy
Idaho Operations Office
Under DOE Contract No. DE-AC07-76ID01570

---

a. ESA, Inc., 836 Clair View Lane, Idaho Falls, ID 83402

ABSTRACT

Recent inspection of the TMI-2 core-former baffle walls (vertical), former plates (horizontal), and lower plenum has been conducted to assess potential damage to these structures. Video observations show evidence of localized melt failure of the baffle walls, whereas fiberoptics data indicate the presence of resolidified debris on the former plates. Lower plenum inspection also confirms the presence of 20 tons or more of core debris in the lower plenum. These data indicate massive core melt relocation and the potential for melt attack on vessel structural components. This report presents analyses aimed at developing an understanding of melt relocation behavior and damage progression to TMI-2 vessel components. Thermal analysis indicates melt-through of the baffle plates but maintenance of structural integrity of the former plates and lower head. Differences in the damage of these structures is attributed largely to differences in contact time with melt debris and pressure of water.

CONTENTS

FIGURES

TABLES

THERMAL INTERACTION OF CORE MELT DEBRIS WITH THE TMI-2 BAFFLE, CORE-FORMER, AND LOWER HEAD STRUCTURES

1. INTRODUCTION

As early as February 1985[1] and again during July 1985,[2] video inspections of the TMI-2 lower plenum indicated that upward of 20 tons or more of the core material relocated to the lower plenum. Debris retrieval from the lower plenum indicates that much of the debris was initially molten. In February 1987, the volume space between the core-former baffle plates and the core barrel was inspected for the presence of fuel debris, using a fiberscope.[3] Results indicate the presence of perhaps several tons of core material in this volume space, much of which may be fused to the horizontal former plates.

These findings heighten the issues of melt progression and the potential for degradation of the core-former assembly (CFA)[a] and lower head, owing to thermal attack by hot relocating "corium" melt. Specifically, questions remain as to the sequence of events leading to corium melt migration, and the consequences and implications of melt interaction with core support structures. This report presents analyses aimed at assessing thermal damage potential to the core-former assembly, and direct thermal attack on the lower head by melt impingement during debris relocation. The report is structured as follows. A brief description is presented of a plausible sequence of events which may have led to migration of core melt debris to the lower plenum. This is followed by a summary of what is currently known of the damage characteristics and observations of corium melt interaction with the core-former and baffle plate structures, as well as the lower plenum. Analyses are then presented

---

a. The core-former assembly (CFA) consists of vertical baffle plates adjacent to peripheral fuel assemblies and a series of attached horizontal former plates. Both are forged from stainless steel, and together form an inner wall of structural material that shrouds the active core region.

concerning molten corium interactions with these structures. Conclusions are drawn relative to degradation of structural integrity of the core-former assembly and lower head.

2. SEQUENCE OF EVENTS LEADING TO CORE DEBRIS RELOCATION

Various investigations have attempted to reconstruct the TMI-2 accident sequence and resultant core damage scenario.[4-7] What is of particular interest is the events that resulted in molten core debris breakout from the uncoolable upper portion of the debris bed, and the attendant potential for molten corium thermal attack on the vertical baffle plates shrouding the core periphery, the attached horizontal core-former plates, and the lower head during melt migration.

The most recent analyses[6-8] indicate that core uncovery, which started about 110 min after reactor scram, was caused by loss of coolant through the pressurizer relief valve. By about 140-150 min, the core is thought to have heated to temperatures sufficiently high that the fuel rods ballooned and ruptured, and most of the uncovered portion of the control rods melted. By 170 min, the upper 40 to 60% of the unoxidized fuel rod cladding is thought to have melted, with attendant partial dissolution of fuel (at the eutectic α-Zr(O)/UO_2 melt temperature of about 2170 K). A temporary restart of the primary coolant 2B-pump occurred at 174 min. As a consequence of coolant injection at this time, the oxidized upper regions of the core are thought to have experienced quench-induced fuel rod shattering and fragmentation, forming a loose rubble bed.

The TMI-2 core damage sequence up to the time of debris bed formation is consistent with separate effects fuel damage experiments regarding fuel rod damage, fuel liquefaction, and molten Zircaloy relocation under reflood conditions. However, some uncertainty exists on core damage progression after the 2B-pump event. The cooling effect of the 2B-pump restart was transitory, and it is likely that the peripheral fuel assemblies experienced temporary cooling, while the inner region of the debris bed remained in an uncoolable configuration. Figure 1 illustrates a best-estimate damage state of the core prior to and just after the 2B-pump transient at 174 min.[8]

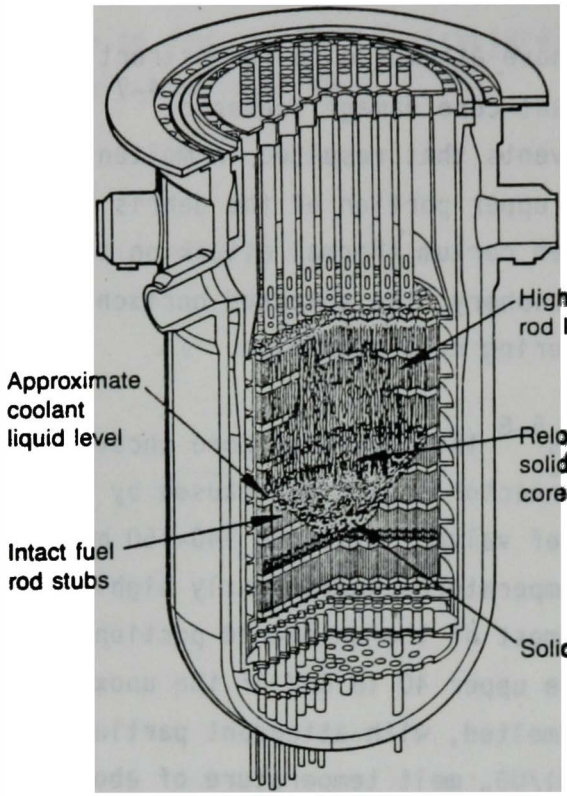

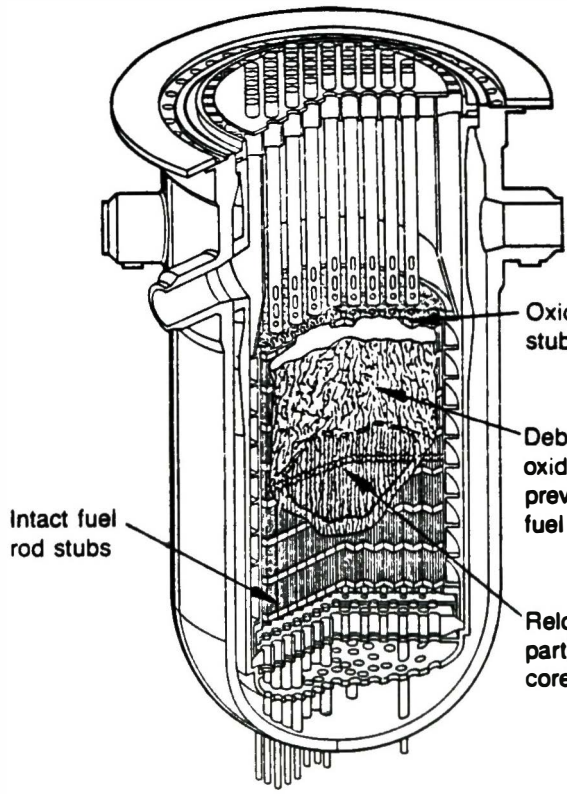

Figure 1. Damage state of the TMI-2 core (a) just prior to and (b) after 28-pump transient.

At 200 min, high-pressure emergency core cooling (ECC) water was injected into the reactor core, over a period of about 17 min.[8] Analysis of thermal hydraulic data (hot and cold leg temperatures, system pressure, and pressurizer response) indicate that the reactor vessel was largely filled by about 207 min,[9] with a significant contribution of the coolant inventory estimated to have come from coolant drainage of the pressurizer as the RCS pressure decreased. However, the consolidated/agglomerated region remained uncoolable after vessel reflood, and was thus subject to continued heatup and eventual melt-breakout. The reactor vessel downcomer and hot legs are predicted to have been only partially filled with liquid coolant after ECC injection, the remainder being exposed to a steam/hydrogen gas mixture.

As discussed in Reference 7, the thermocouples in the peripheral assemblies responded to ECC vessel reflood, but the thermocouples in the central assemblies remained in a high-temperature-alarm state. It is believed that the central thermocouples formed relocated junctions within the consolidated region and were thermally shielded from the cooling water. Analysis[6] of the degraded core heatup indicates that by 225 min, approximately 12,000 kg of core material inside the central degraded core region (or greater, depending on the axial temperature gradient assumed) could have remelted from decay heat.

At about 225 min, several simultaneous events indicate a major change in core configuration. Many of the in-core self-powered neutron detectors (SPNDs) alarmed. Examination of the alarm data show that the alarms first went off in the east quadrant of the core and then propagated toward the center.[7] Some of the core exit thermocouples also alarmed at this time, following a similar sequence as the SPNDs, that is, starting from the east quadrant and propagating toward the core center. The count rate of a neutron source-range monitor located on the outside of the reactor vessel also increased sharply at 225 min, and then decayed slowly. Likewise, a primary system pressure pulse of about 2 MPa was recorded at 225 min, and the temperature in the cold leg (A-loop) piping increased by as much as 80 K in 12 s. The source-range monitor response, the primary system

pressure, and the cold leg temperature data are shown in Figure 2. The discovery of core material in the lower plenum, core examination data indicating the apparent flow path of molten material in the east quadrant of the core,[8] together with the data shown in Figure 2, present strong evidence that molten material relocated to the lower plenum at about 225 min.

Although the exact details of corium melt relocation to the lower plenum are open to conjecture, the above sequence of events appears reasonable in light of available data. After the major relocation event, around 225 min, there was little indication of another major core configuration change. The current best-estimate end-state condition[8] of the damaged TMI-2 core is illustrated in Figure 3.

In light of the current state of knowledge regarding corium melt relocation at ≈225 min (primarily on the east quadrant) and evidence of fuel debris entrapment in the volume space between the core baffle plates and barrel, an investigation was initiated to assess the potential for corium melt attack on core support structures. Specifically, core melt interaction with the core-former and baffle plate structures are addressed, as well as the effects of corium melt impingement on the lower head. Evidence of core-former, baffle plate, and lower head damage are presented in Section 3, while thermal analysis of such structures is given in Sections 4, 5, and 6. Discussion of results and conclusions are then presented in Section 7.

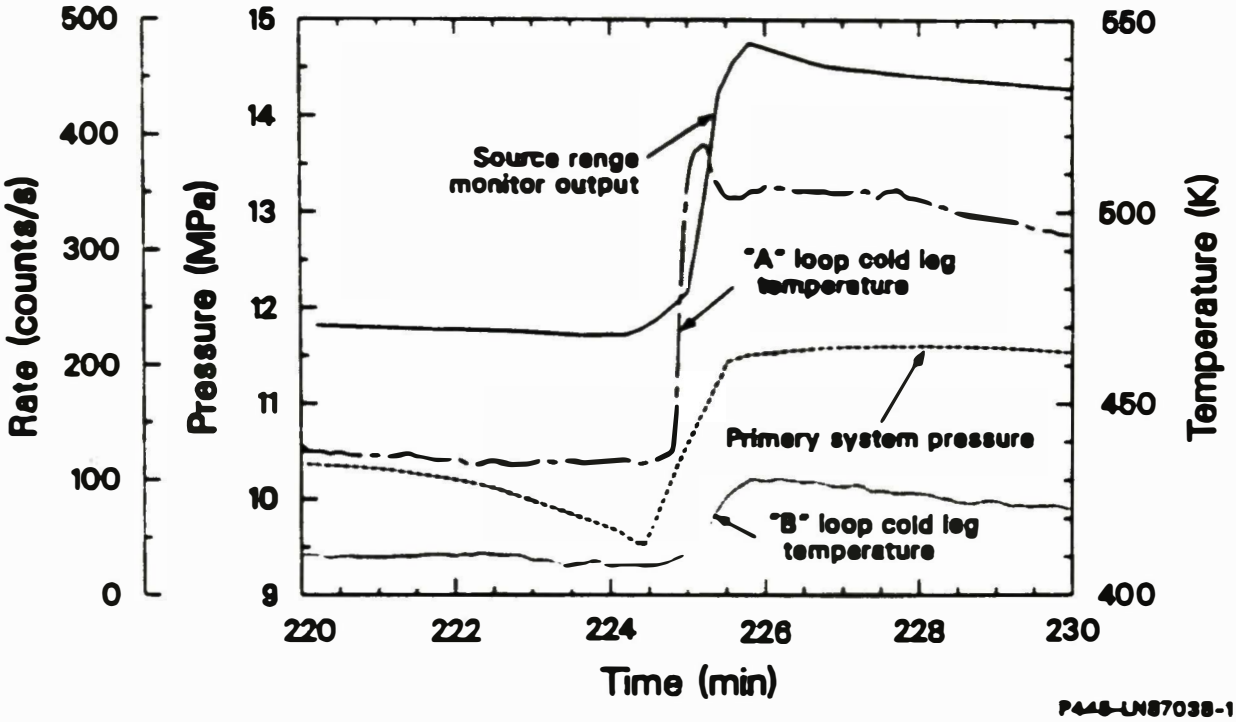

Figure 2. Source-range monitor response, primary system pressure, and cold-leg temperatures at approximately 225 min.

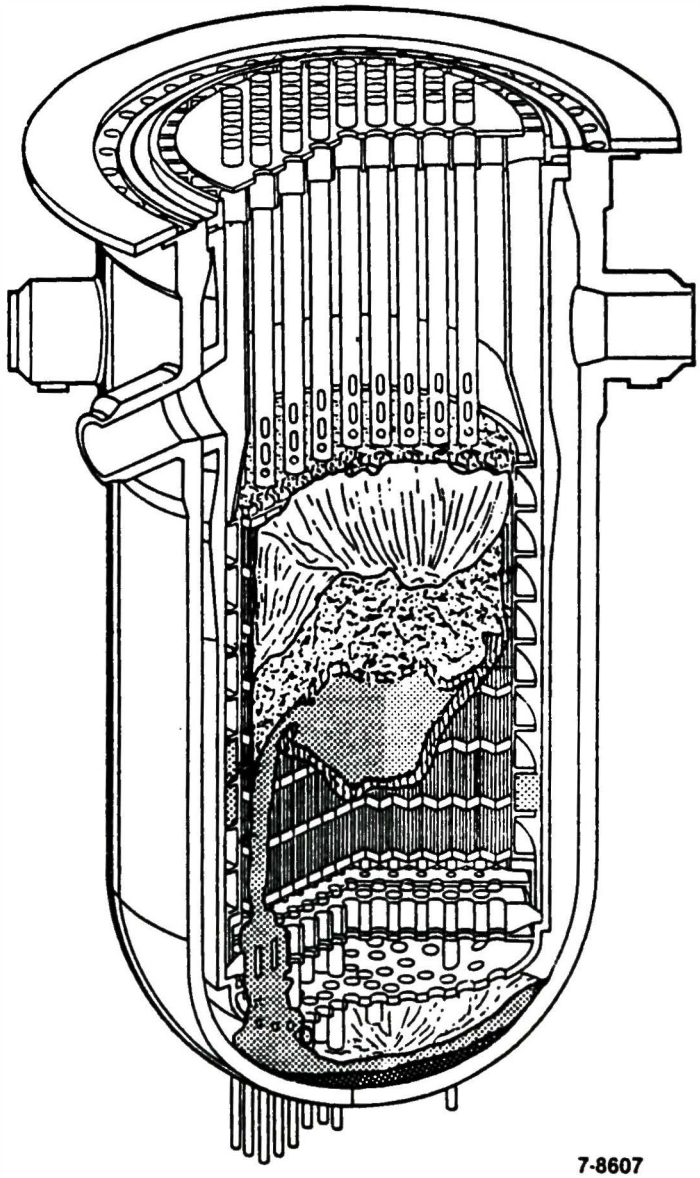

Figure 3. TMI-2 known end-state core configuration.

3. EVIDENCE OF BAFFLE PLATE, CORE-FORMER, AND LOWER PLENUM DAMAGE

Baffle plate, core-former, and lower plenum damage characterization are summarized here, based on information obtained from recent reactor vessel inspection, namely

- Video camera inspection of, and debris retrieval from, the lower plenum[10-13]

- Video camera inspection of the inside surface of the vertical baffle plates[14] shrouding the core periphery

- Fiberscope inspection of the horizontal core-former plates, which act as a spacer between the baffle plates and core barrel.[3]

First however, a brief description is presented of the geometric configuration of the core-former assembly (CFA), which encompasses the core-former and baffle plate structures. A description of lower plenum structures is given in Reference 15, so will not be repeated here.

3.1 Reactor Vessel Internal Structures

Figure 4 presents a cross-sectional view at the TMI-2 core midplane. The reactor vessel internals include the active core, plenum, and core-support assemblies. The outermost components of the vessel internals consist of the vessel wall, stainless-steel liner, coolant downcommer space, stainless-steel thermal shield, shield/core-barrel annular gap space, and core barrel (or core support assembly-CSA) and baffle plates. Within the annular gap space between the core barrel and baffle plates (which shroud the core periphery) are a series of horizontal former plates. Table 1 gives their appropriate dimensions. Of interest here are the structural characteristics of the vertical baffle and horizontal core-former plates, which appear to have suffered damage caused by thermal attack from molten corium debris.

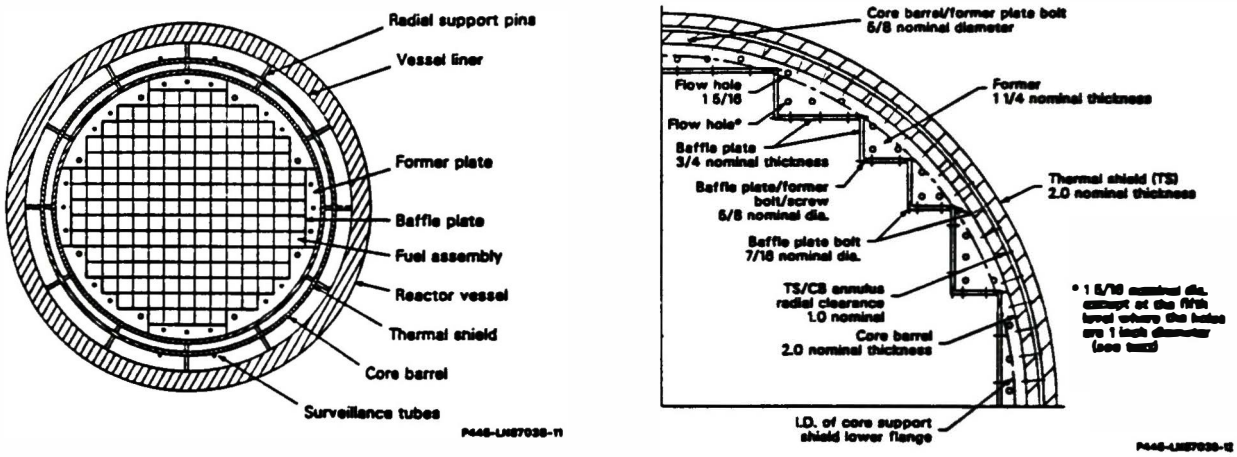

Figure 4. Illustration of reactor vessel internal structures.

TABLE 1. DIMENSIONAL CHARACTERISTICS OF THE CORE FORMER, BAFFLE PLATE, AND CORE SUPPORT ASSEMBLY

Parameter	Units	Value	Comment
Baffle Plates			
Geometry	--	--	Vertical rectangular plates
Length	in.	166 ~ 3	--
Width	in.	8.6/17.2/43.0	--
Thickness	in.	0.9 ~ 0.3	Approximate
No. plates	--	24/8/4	Total
Material	--	Stainless steel	--
Stainless Steel	lb	22,250 ± 10%	all plates together
Former Plates			
Geometry	--	--	Horizontal/perforated
Total area	ft^2	17.8	1 elevation, 1 side
Flow area	ft^2	1.4 ± 0.4	1 elevation, perforations
Thickness	in.	0.9 ± 0.3	Approximate
No. plates	--	8	No elevations
Material	--	Stainless steel	--
Stainless steel	lb	4,940 ± 10%	All elevations
Core Support (Barrel)			
Geometry	--	--	Cylindrical
Length	in.	166 ± 3	--
O.D.	in.	245.0	--
I.D.	in.	141.2	--
Material	--	Stainless steel	--
Stainless steel	lb	40,930 ± 10%	--
Flow Areas			
Between baffle plates and core barrel	ft^2	17.8 ± 10%	Annular gap space
Through holes in former plates	ft^2	1.4 ± 50%	At 1 elevation

The core-former assembly (CFA) consists of the vertical baffle plates adjacent to peripheral fuel assemblies and the attached horizontal former plates. Both are forged from stainless steel and together form an inner wall of structural material that laterally encloses the active core region. Eight horizontal former plates are axially spaced between the bottom and top of the active core region. Flow holes in the horizontal former plates allow for a small portion of the primary coolant to flow upward, in the 5-in. space between the baffle plates and the inside wall of the core barrel. The vertical baffle plates lie flat against the outside faces of the peripheral fuel assemblies. Appendix A details design features of the baffle and former plates.

3.2 Video Inspection of the Vertical Baffle Plates

Video inspection of standing peripheral fuel assemblies was conducted on February 8, 1987.[14] Various degrees of assembly damage were noted, from relatively undamaged fuel rods to heavily oxidized and broken rod stubs. The grid spacers and end fittings also showed some damage. Details of the damage state of various assemblies are discussed in Reference 14. What is of interest here is the damage noted in the east quadrant of the reactor vessel, where a region of the core baffle plate was inspected.

Video data (see Reference 3) indicate apparent melt-through of an east-quadrant baffle plate, as viewed from inside the core in the vicinity of core grid location R6/P5. Details of damage to this baffle plate are shown in Figure 5, taken from still frames of the video tape. A melt-through hole about 8-in. long and a maximum width of about 3-in. is indicated. Fuel rod remnants appear to lie inside the undercut region of the hole.

Upon removal of the peripheral fuel assemblies from the TMI-2 core, the baffle plates were reexamined in June 1987. Video examinations

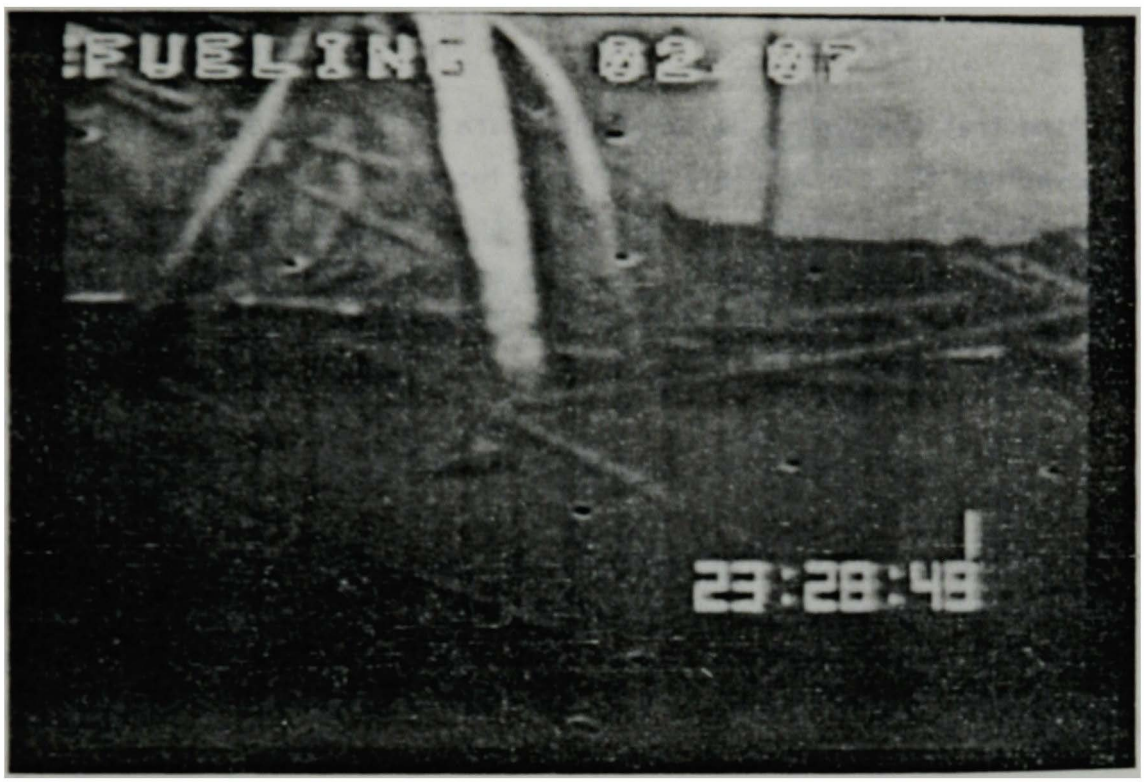

Figure 5. Evidence of melt ablation of an east-quadrant baffle plate.

confirmed the pressure of several melt-through holes in the east quadrant. These baffle plate melt-through data[16,17] are summarized below:

Grid Location	Hole Dimensions	Elevation
P5	8 in. x 3 in.	303 ft 8 in.
R6	8.5 in. x 1.5 in.	303 ft 8 in.
R6	9 in. x 1 in.	303 ft 8 in.

Noting that the bottom of the active core is located at about the 299-ft elevation, the baffle plate holes are located at approximately 4.75 ft from the bottom of the core. The coincidence of east-quadrant melt relocation data (see Section 2) and baffle-plate melt-through, suggests that baffle plate damage may have occurred as a consequence of major melt relocation to the lower plenum.

3.3 Fiberscope Inspection of Horizontal Former Plates

In late February 1987, the volume space between the core baffle plates and the core support assembly (barrel) was inspected for the presence of fuel debris, using a fiberscope.[3] The fiberscope was inserted through a guide pipe into the holes in the core-former plates at various locations. There are 80 such holes in each of 8 horizontal former plates.[a] Inspections were performed in 9 holes.

An elevation view showing each of the 8 core-former plates is shown in Figure 6. As the fiberscope was inserted to lower elevations, it eventually encountered blockages in every position. The blockages prevented the fiberscope from being inserted to lower elevations.

Table 2 summarizes the location of the blockages at each position inspected, whereas Figure 7 shows a view of core-former blockage with the cylinder flattened into a plane. Results show that the highest elevation

---

a. At a hole diameter of 1.75 in., the flow area per hole is 2.4 in^2. At 80 holes per elevation, the total flow area is 192 in^2 (1.34 ft^2), which compares with the 1.4 ft^2 given in Table 1.

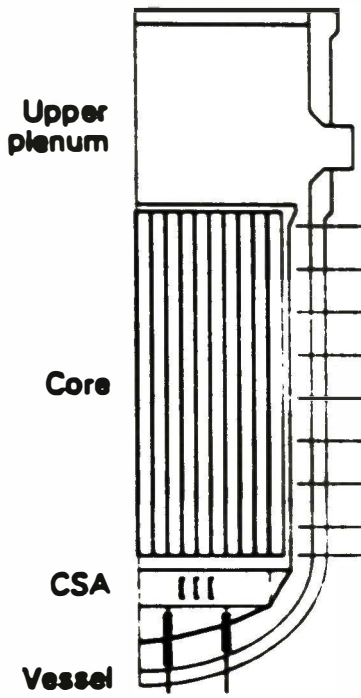

	Inches above fuel stack bottom	Elevation	
Plate 1	147.4	311' 3"	
Plate 2	129.4	309' 9"	18"
Plate 3	111.4	308' 3"	18"
Plate 4	93.4	306' 9"	18"
Plate 5	71.4	304' 11"	22"
Plate 6	49.4	303' 1"	22"
Plate 7	24.4	301' 0"	25"
Plate 8	0.4	299' 0"	24"
Bottom of lower grid rib section			14"

P446-LN87038-2

Figure 6. Illustration of elevation positions of the 8 TMI-2 core-former plates.

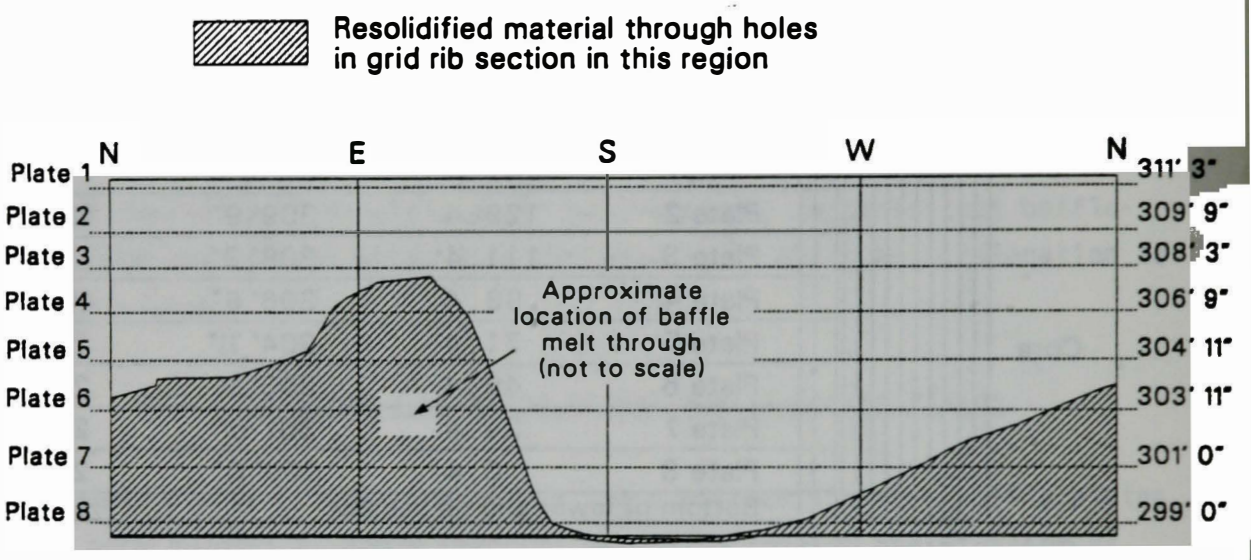

Figure 7. Side-view illustration of blockage elevation data within the core-former volume space, based on fiberscope insertion.

TABLE 2. SUMMARY OF BLOCKAGE CHARACTERISTICS IN THE FORMER-PLATE REGION OF THE TMI-2 CORE SUPPORT ASSEMBLY

Hole Number	Blockage Elevation	Comments
5	298 ft 1 in.	Loose debris in the flow hole in the lower grid section
16	298 ft 6 in.	6 in. below former plate 8
36	303 ft 0 in.	Debris at bottom of former plate 6
45	304 ft 4 in.	Solidified debris partially blocking hole in plate 5 and solid at 7 in. below plate 5
56	304 ft 10 in.	Sample taken here
61	307 ft 6 in.	Fiberscope guide tube forced through loose debris to El. 305 ft 10 in.
65	308 ft 0 in.	Fiberscope guide tube forced through loose debris to El. 306 ft 0 in.
72	304 ft 0 in.	Packed loose debris
76	299 ft 1 in.	Hard stop at this elevation

of the debris resting on the core-former plates is in the east quadrant. Also shown in the approximate location of the baffle plate melt-through hole. This is consistent with the east-quadrant relocation scenario discussed in Section 2.

Based on the blockage findings presented in Figure 7, an estimate was made of the amount of core debris within the former plate region. Assuming that everything below that surface is filled with loose debris of an average density of 4.5 g/cc, it is estimated that as much as 13,600 lb of core debris may be fused to or resting on the horizontal core-former plates.[17]

3.4 Inspection of Lower Plenum

Various lower-plenum inspection efforts have confirmed the presence of 20 tons or more of core debris in the lower plenum[10-13] and thermal damage to two stainless-steel instrument guide tubes.[11] Instrument guide tube 45, at core grid location R-7, suffered the most significant damage noted to date. The apparent thermal damage has completely melted away the eastern side of this guide tube. Core debris material that had accumulated around the bottom portion of this guide tube was later removed, which exposed the lower regions of the guide tube. Inspection showed that melt damage extended to about 9 in. above the bottom end of the stainless-steel guide tube. The Inconel nozzle, which is sleeve fitted into the guide tube, was visible and also appears to have experienced melt damage. The instrument string inside the nozzle also appears to have suffered severe melting.

Previous analysis of lower plenum structural damage,[16] indicate that melt failure of Inconel instrument nozzles could have occurred at localized hot-spot regions, caused by the limited thermal capacity of the Inconel nozzle (wall thickness ≈0.69 in.) and its relatively low melting point (≈1600 K). Thus, recent lower plenum inspection appears to support results from prior analysis.[15]

Thermal analysis[15] of corium-melt attack on the lower head, also indicates that the stainless-steel liner is not likely to have experienced melting upon initial contact with either metallic (molten steel or Ag-In-Cd melt) or ceramic fuel debris. The geometry considered was that of corium melt spread uniformly over the bottom head. However, the recent update of the melt relocation scenario indicates that the major fraction of melt relocation occurred in the east-quadrant of the vessel, where drainage may have occurred over several minutes. The question, thus, arises as to whether localized melt attack of an impinging jet on the lower head could have resulted in localized melt ablation of the liner. This question is investigated in Section 6.

Observations from the various TMI-2 vessel inspection efforts heighten the issues of melt progression and the potential for degradation of core-former assembly (CFA) and lower-head structural integrity. Specifically, questions remain as to the consequences and implications of corium melt interaction with the core-former assembly (CFA) and lower head. Analyses are therefore presented in subsequent chapters, aimed at assessing thermal interaction behavior of corium melt with the baffle and core-former plates, as well as the potential for melt ablation of the lower head caused by thermal attack by an impinging jet of molten corium.

4. DEBRIS THERMAL ATTACK ON THE VERTICAL BAFFLE PLATES

Within this chapter, analyses are presented to assess the potential for, and conditions associated with, baffle plate melt-through. Of primary interest is a definition of corium melt characteristics (metallic or ceramic) which leads to melt ablation of the baffle plate, and determines the time required for baffle melt-through.

4.1 Instantaneous Contact Temperature

Since the baffle plates are made of relatively low-melting-point stainless steel (T_{mp} ≈2500°F = 1640 K), and since the plate thickness is 0.75 in., melt ablation of the baffle plates by the relocating molten corium is a distinct possibility. An evaluation of the thermal conditions leading to stainless-steel baffle melting can be assessed from consideration of the contact situation illustrated in Figure 8. The configuration shown is one of molten corium in good surface contact with the baffle plate, where both materials are assumed to be of infinite thickness. For semi-infinite geometry, the contact temperature at the interface can be expressed as[18]

$$T_I = \frac{T_H(k/\alpha^{0.5})_H + T_C(k/\alpha^{0.5})_C}{(k/\alpha^{0.5})_H + (k/\alpha^{0.5})_C}$$

where T is temperature, k is thermal conductivity, α is thermal diffusivity, and the subscripts H and C refer to the hot corium and cold baffle respectively.

Calculational results are presented in Table 3 for ceramic-like corium assuming UO_2 thermal properties. Owing to the higher thermal conductivity of stainless steel compared to UO_2, the interface temperature is closer to the bulk temperature of the baffle plate. Since the melting point of stainless steel is about 2500°F (1644 K), initial melting of the baffle plate is not inferred for ceramic-like core debris.

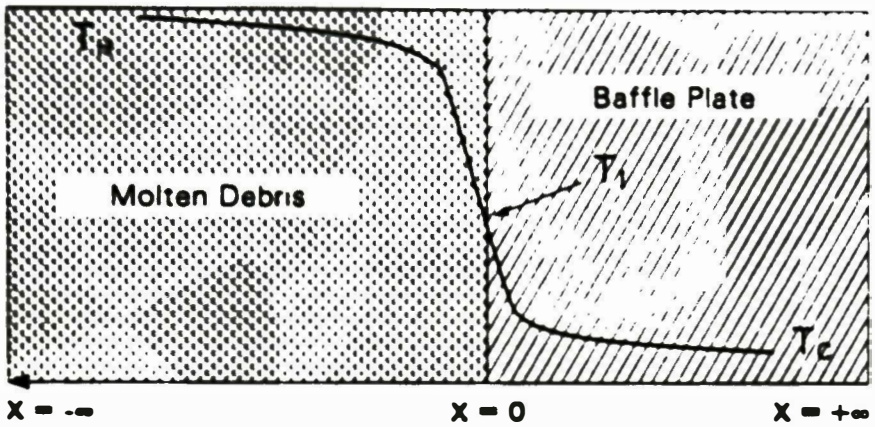

P445-LN87040-4

Figure 8. Illustration of two semi-infinite slabs at different bulk temperature, and the instantaneous contact temperature at the surface of separation.

TABLE 3. ESTIMATE OF CONTACT INTERFACE TEMPERATURE BETWEEN UO_2 DEBRIS AND TMI-2 CORE-FORMER BAFFLE PLATE

Governing Equation

$$T_I = \frac{T_H(k/\alpha^{0.5})_H + T_C(k/\alpha^{0.5})_C}{(k/\alpha^{0.5})_H + (k/\alpha^{0.5})_C}$$

Parameter Values

H = UO_2 Properties	C = Stainless-Steel Properties
k_H = 2.1 Btu/h-ft-°F	k_C = 9.4 Btu/h-ft-°F
α_H = 0.032 ft^2/h	α_C = 0.157 ft^2/hr
$k/\alpha^{0.5}$ = 11.8	$k/\alpha^{0.5}$ = 23.7
T_{mp} = 4670°F (2850 K)	T_{mp} = 2500°F (1644 K)

Assumption

Assume that the core-former baffle plate is at the saturation temperature of water, corresponding to a pressure of 1500 lb/in^2, i.e. T_C = 596°F (586 K)

Calculation

T_H, °F (K)	T_I, °F (K)
4000 (2477)	1887 (1304)
4500 (2755)	2068 (1404)
5000 (3033)	2250 (1505)
7000 (4144)	3996 (2475)

Table 4 presents a similar calculation, where in this case the corium is considered to be a mixture of U-Zr-O components, with an effective metal-like conductivity of 50 W/m-K (28.9 Btu/h-ft-°F). This increase in debris thermal conductivity results in a higher interface temperature, which partitions between that of the corium and baffle plate temperatures. For metallic-like debris, surface melting of the baffle plates at corium temperatures in excess of ≈3600°F (2255 K) is estimated.

Note that the contact temperature is based on the assumed geometry of <u>two semi-infinite</u> regions of different properties and bulk temperatures. As such, the solution is valid only until the thermal front penetrates the thickness of either, whereupon the bulk material begins to heat up (or cool down), with a corresponding change in interface temperature. Thus, the above estimate is simply an indication of the <u>initial-contact</u> temperature.

4.2 Time for Baffle Plate Melting

In reality, the baffle plate has limited thickness, so that a closer representation of the true geometry is similar to that illustrated in Figure 9. In Figure 9 the baffle plate is represented by a wall of finite thickness, in contact with a corium melt of infinite thickness. Assuming one-dimensional heat transfer in the x-direction, the problem can be approximated as a semi-infinite material (region-1) in contact with a material of different conduction properties and of finite thickness (region-2). Neglecting the decay-heat source term in region-1, the heat conduction equation in each region can be written as

$$\frac{dT(x,t)}{dt} = \alpha \frac{d^2T(x,t)}{dx^2}$$

where T is the temperature, α is the thermal diffusivity, t is the time variable, and x is the spatial variable. The general form of the solution for semi-infinite geometry can be expressed in terms of a series expansion of the error function,[18] that is,

TABLE 4. ESTIMATE OF CONTACT INTERFACE TEMPERATURE BETWEEN U-Zr-O DEBRIS AND TMI-2 CORE-FORMER BAFFLE PLATE

Governing Equation

$$T_I = \frac{T_H(k/\alpha^{0.5})_H + T_C(k/\alpha^{0.5})_C}{(k/\alpha^{0.5})_H + (k/\alpha^{0.5})_C}$$

Parameter Values

H = U-Zr-O Properties	C = Stainless-Steel Properties
k_H = 29.0 Btu/h-ft-°F	k_C = 9.4 Btu/h-ft-°F
α_H = 0.45 ft^2/h	α_C = 0.157 ft^2/hr
$k/\alpha^{0.5}$ = 43.2	$k/\alpha^{0.5}$ = 23.7
T_{mp} = 2170 K = 3447°F	T_{mp} = 1644 K = 2500°F

Assumption

Assume that the core-former baffle plate is at the saturation temperature of water, corresponding to a pressure of 1500 lb/in^2, i.e. T_C = 596°F (586 K)

Calculation

T_H, °F (K)	T_I, °F (K)
3000 (1922)	2148 (1449)
3600 (2255)	2535 (1663)
4000 (2477)	2794 (1807)
5000 (3033)	3440 (2166)

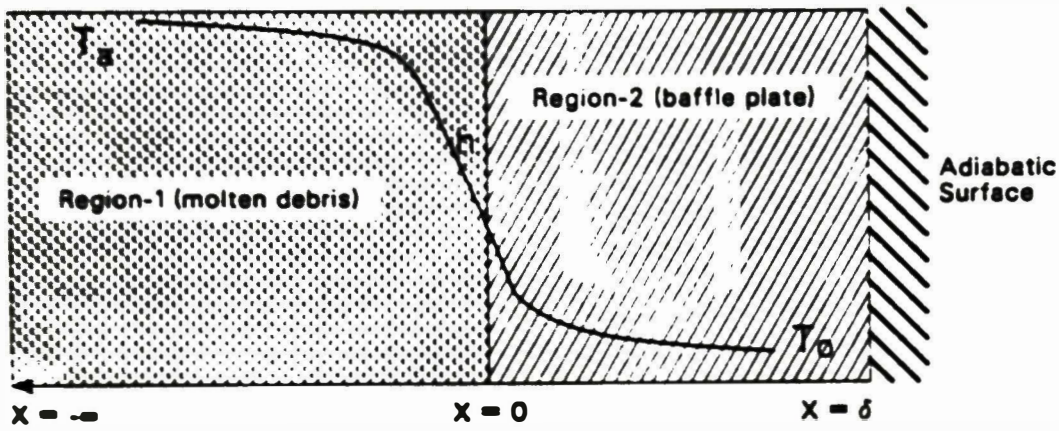

P445-LN87040-5

Figure 9. Illustration of a semi-infinite melt region in contact with a solid wall of finite thickness (δ), insulated at the ouside surface (x = δ).

$$T(x,t) = A \sum_{n=0}^{n=\infty} B^n \, \mathrm{erf}[nx/(\alpha t)^{0.5}]$$

where the constants A and B are functions of the properties and boundary conditions of the particular problem at hand.

For transient heat conduction in simple shapes subject to boundary conditions of practical importance, the temperature-distribution solutions have been calculated and the results are available in the form of charts or tables. For present purposes, the core debris region can be considered a semi-infinite slab at a bulk constant temperature (T_a), with a constant heat transfer coefficient (h) at the contact surface between the debris and baffle plate. The baffle plate is of thickness δ, and is assumed to be insulated (adiabatic) at the surface, $x = \delta$.

The chart presented in Figure 10 (Reference 19) yields the solution to transient heatup of the baffle plate, as a function of the dimensionless Fourier (Fo) and Biot (Bi) numbers. The Biot number is the ratio of the convective-to-conductive thermal resistance, and F_o is the ratio of thermal penetration distance to the wall thickness, that is,

$$Bi = h\delta/k$$

$$Fo = \alpha t/\delta^2 \quad .$$

As indicated, the Biot number is governed by the conductivity of the wall material and the heat transfer coefficient (h) at the contact surface. The conductivity of the stainless steel is known; however, the heat transfer coefficient (h) depends on the characteristics of the melt debris. For present purposes, it can be assumed that the conduction properties of the molten corium are dominant, so that the Biot number reduces to the conductivity ratio, that is,

$$Bi = k_1/k_2 \quad .$$

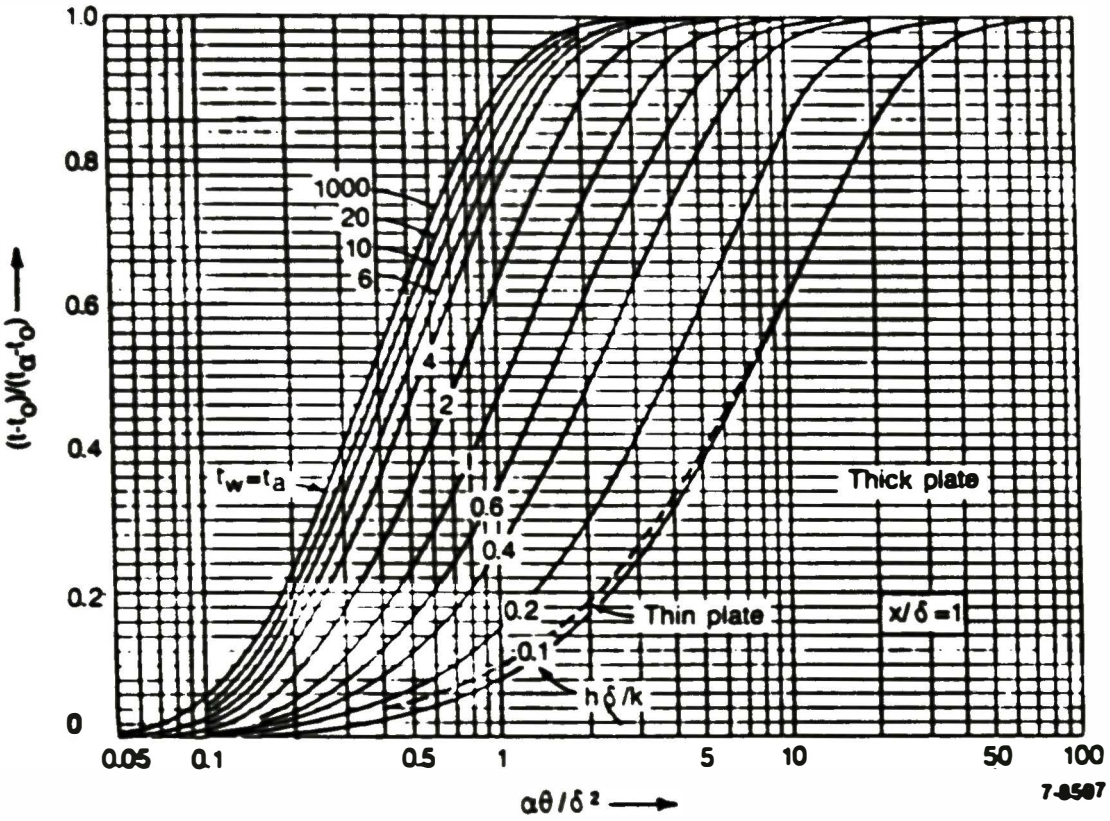

Figure 10. Temperature response of an insulated, thick plate ($0 \leq x \leq \delta$) at $x/\delta = 1$ after sudden exposure to a uniform convective environment.

Parameter values are estimated in Table 5, indicating the approximate numerical values of the dimensionless groups for baffle plate heatup to the melting point of stainless steel (2500°F) for two debris temperatures, namely at the α-Zr(0)/UO_2 eutectic (2150 K) and UO_2 (2850 K) melt temperatures:

$$Bi = h\delta/k = 0.22$$

$$T' = 0.68 \text{ (at } \alpha\text{-Zr(0)/}UO_2 \text{ eutectic temperature)}$$

$$T' = 0.47 \text{ (at } UO_2 \text{ melting point)} \quad .$$

Making use of Figure 10, the associated Fourier numbers are estimated to be

$$Fo \text{ (at } T' = 0.68) = \alpha t/\delta^2 = 6.0$$

$$Fo \text{ (at } T' = 0.47) = \alpha t/\delta^2 = 3.5 \quad .$$

Thus, the time for the baffle plate thickness ($x/\delta = 1$) to reach the stainless-steel melting point is estimated to be

$$t = 6\delta^2/\alpha = 6(0.0625 \text{ ft})^2/(0.1567 \text{ ft}^2/\text{hr}) = 0.15 \text{ hr (9 min)}$$

$$t = 3.5\delta^2/\alpha = 3.5(0.0625 \text{ ft})^2/(0.1567 \text{ ft}^2/\text{hr}) = 0.087 \text{ hr (5 min)}$$

or approximately 5 to 10 min.

In the above solution, the analytic complexities associated with a moving phase-transformation front were neglected. For the corium melt region, convective currents allow for agitation of the melt, so that any potential solid crust buildup is unstable and dissolved in the melt. However, a moving phase boundary (melt front) exists within the baffle plate, which has not been accounted for in the above analysis.

As discussed in References 20 through 23, the exact analytical solutions to most problems of transient-heat conduction with a moving

TABLE 5. THERMOPHYSICAL AND HEAT-TRANSFER PROPERTIES STAINLESS-STEEL BAFFLE PLATES

Thermophysical Properties of Baffle Plate (Stainless-Steel)

T_{mp} = 2500°F = 1640 K

C_p = 0.12 B/lb°F = 0.12 cal/g K

k = 9.4 Btu/h-ft-°F = 16.26 W/m-K

$\rho = 0.29 \frac{lb}{in.^3} = 500\ lb/ft^3 = 80\ kg/m^3$

$\alpha = k/\rho C_p = 9.4/500\ (0.12) = 0.157\ ft^2/h$

L (Fe) = 65 cal/g = 117 B/lb

Convective Heat Transfer Coefficient, h

$h = k_1/a_1$

k_1 = UO_2 thermal conductivity = 3.66 W/m-K = 2.1 B/lb ft-°F

a_1 = 0.75 in. = 0.0625 ft

$h = 2.1/0.0625 = 33.6\ B/lb\ ft^2 °F$

Biot Number, Bi

$Bi = h\ \delta/k_2 = k_1/k_2$

Bi = 33.6(0.0625)/9.4 = 0.22

Temperature Ratio, $T-T_o/T_a-T_o = T'$

T = melting point of stainless steel = 2500°F

T_a = core debris temperature

T_o = initial temperature of baffle plate = water saturation temperature at 1500 psi ≈600°F

$T-T_o/T_a-T_o = 2500-600/T_a-600$

TABLE 5. (continued)

Case 1

T_a = α-Zr(O)/UO_2 eutectic melt temperature = 2150 K = 3410°F

T' = 0.68

Case 2

T_a = UO_2 melting point = 2850 K = 4670°F

T' = 0.47

phase-transformation boundary are not readily obtainable. This is due to the always-present nonlinearity of the moving melt front. The only exact analytic solutions to the transient freezing problem are those for a semi-infinite slab, with a constant temperature at the cooling surface. There are no exact solutions for other boundary conditions, such as constant heat flux or radiation. Various approximate techniques, however, are available, including the integral heat balance[22] and bounds averaging methods.[22,23] However, the simplest technique has been suggested by London and Saben,[24] where an effective heat capacity ($C_{p,e}$) is specified so that nonlinearity of the problem is avoided and the single-phase transient solution is employed, where

$$C_{p,e} = C_p + [L/\Delta T]$$

In this expression, ΔT is the temperature difference between the melting point and the initial temperature, and L is the heat of fusion.

As indicated, the heat capacity of the material is increased to account for the added heat of fusion involved in melting. This technique is used here to account for solid-to-liquid phase transformation in the baffle plate, where the effective heat capacity for melting of stainless-steel (see properties in Table 5) is

$$C_{p,e} = \frac{0.12\ B}{lb°F} + \left[\frac{117\ B/lb}{2500°F} = 0.047\ B/lb°F\right] = 0.167\ B/lb°F \quad .$$

Accounting for the heat of fusion effectively adds 0.047 B/lb °F to the single-phase heat capacity. Using this effective specific heat, an effective diffusivity (α_e) is also estimated, based on property values given in Table 5 for k and ρ, that is

$$\alpha_e = k/\rho C_{p,e} = 9.4/500(0.167) = 0.113\ ft^2/h \quad .$$

As can be seen, an increase in specific heat results in an delayed time for complete melt-through of the 3/4-in. thick baffle plate, that is,

$$t(\text{at } T' = 0.68) = 6\delta^2/\alpha_e = 6(0.0625 \text{ ft})^2/0.113 \text{ ft}^2/\text{h}) = 0.21 \text{ h } (12 \text{ min})$$

$$t(\text{at } T' = 0.47) = 3.5\delta^2/\alpha_e = 3.5(0.0625 \text{ ft})^2/0.113 \text{ ft}^2/\text{h}) = 0.21 \text{ h } (7 \text{ min})$$

as compared to 5-10 min, ignoring heat of fusion effects.

In addition to heat of fusion effects, cooling of the baffle at the outer surface will also delay somewhat the time for plate melt-through. However, for good core melt/baffle plate contact, conduction at the inside surface will generally override convective or radiative heat transfer at the outer surface of the baffle plate. Likewise, total melt front penetration of the entire 3/4-in. thickness would not be required for loss of integrity of the baffle plate structure. Thus, melt failure of the baffle plate caused by contact with molten corium is predicted to occur on the order of about 15 min.

Melt failure of the baffle plate will lead to debris relocation through the volume space between the baffle and core barrel walls, which also contains a series of eight horizontal stainless-steel core-former plates. Melt debris relocation through the baffle-plate melt holes and molten corium attack on the core-former plates are assessed in the following chapter.

5. DEBRIS THERMAL ATTACK ON HORIZONTAL CORE-FORMER PLATES

As discussed in Section 3, approximately 13,600 lb (≈6170 kg) of core debris is estimated to have accumulated on the horizontal core-former plates. Video inspection through melt holes in the east-quadrant baffle plates also indicates that much of this debris appears to have resolidified from a once-molten state.[25] Within this section, analyses are presented to assess melt-debris migration characteristics through the series of eight stacked core-former plates and melt-debris/core-former plate thermal interaction.

5.1 Melt-Debris Relocation Behavior

Each of the core-former plates have 80 flow holes that are 1-5/16 in. in diameter and are aligned top to bottom (see Appendix A). The fifth-level (mid-core height) plate, however, has 16 holes at 1 5/16 in. diameter and 64 holes at 1 in. diameter. The mid-level (5th) plate, thus, fixes the minimum flow area for debris migration through the former plates. The vertical baffle plates also contain holes, which are approximately 1-3/8 in. in diameter. A typical row of baffle holes is located below a corresponding row of bolts that attach the baffle plates to the former plates. The number of holes range from 80 to 32 holes per row around the baffle circumference.

As shown in Figure 7, the east-quadrant melt-through holes (observed to date) are located at an elevation of about 4.75 ft from the bottom of the active core, whereas the fiberscope data indicate debris blockages at a somewhat higher elevation. It would be expected that molten material would flow laterally across the core-former plates and downward through the flow holes in the former plates. High-elevation debris blockages are, therefore, an unexplained anomaly at this time. More definitive data of debris accumulation on the core-former plates and characterization of the baffle plates are required to explain the presence of debris at elevations above presently known baffle plate melt-through holes. One explanation might be that partial core debris entry into the former plate region occurred through the normal 1-5/8-in. holes in the as-fabricated baffle

plates, while the lower elevation baffle plate melt-through holes provided additional open area for melt penetration into the core-former region.

For the present, debris migration behavior is characterized based upon the combined flow area of the baffle plate as-fabricated, as well as east-quadrant melt-through holes. The potential for lateral melt migration along the surface of the former plates, versus drainage through the former plate flow holes, is first assessed. In addition, a characteristic melt drainage time is estimated, based upon the available hole area of the fifth former plate.

5.1.1 Lateral Migration Versus Drainage Potential

To assess the potential for lateral migration of melt debris along the surface of the core-former plates, a comparison is made of the hole area for melt drainage versus the flow area for outflow of core-melt debris through the baffle plates. As discussed in Appendix A, there are 32 holes (1-3/8 in. in diameter) in the baffle plate region associated with the fifth level former plate. Assuming that outflow of core-melt through the baffle plates occurred only in the east-quadrant (1/4 of core circumference), the available flow hole area of the east-quadrant baffle plate is estimated to be

$$A_{baffle,hole} = \frac{32}{4} \times \left[\frac{\pi}{4}(1.375)^2\right] = 11.88 \text{ in.}^2 \approx 12 \text{ in.}^2 \quad .$$

Noting that a melt-through hole 8 in. long and 3 in. wide (24 in.^{2}) also has been observed in the east-quadrant baffle plate, the potential flow area for melt migration through the east-quadrant baffle plate is estimated to be

$$A_{baffle,hole} = 12 \text{ in.}^2 + 24 \text{ in.}^2 = 36 \text{ in.}^2 \quad .$$

The estimated area for outflow of melt debris through the baffle plate can be compared with the available area for drainage, via the flow holes in the core-former plates. The total flow area of the fifth level plate is

$$A_{former,hole} = 16 \times \left[\frac{\pi}{4}(1.3125)^2\right] + 64 \times \left[\frac{\pi}{4}(1.0)^2\right]$$

$$= 21.65 \text{ in.}^2 + 50.27 \text{ in.}^2 = 71.92 \text{ in.}^2 \quad .$$

The associated flow area of the east-quadrant (1/4 core) former plate is, thus,

$$A_{former,hole} = 71.92 \text{ in.}^2/4 \approx 18 \text{ in.}^2 \quad .$$

On comparing the flow areas, it can be seen that $A_{baffle,hole}$ is greater than $A_{former,hole}$. Since the core-former flow-hole area is insufficient to accommodate mass flow through the available baffle plate flow area, the implication is that some lateral migration of melt debris along the surface of the core-former plate occurred. Lateral migration is supported by observation of debris found on both the north and east quadrants of the core-former plates, as shown in Figure 7.

In addition to estimating the potential for lateral migration, it is also interesting to assess a characteristic drainage time for downward melt migration through the core-former holes.

5.1.2 Melt Drainage time

To assess a characteristic drainage time, the fifth former plate is assumed to be uniformally covered with a layer of core-melt debris, at a height of 22 in., (which is equal to the spacing between the fourth and fifth former plates). The mass flow rate through the former plate holes (of flow area A_f) is considered controlled primarily by gravity, so that the Bernoulli discharge equation applies:

$$\dot{m}_f(t) = A_f C_d \, [2g \, Z(t)]^{0.5}$$

where Z (t) is the melt height, which varies with time (t), and the other parameters are

g = gravitation constant

C_d = discharge coefficient

A_f = flow area.

Applying the continuity equation, the discharge rate is equated to the rate of change of melt resting on the core-former plate, i.e.,

$$A_f C_d \, [2gZ(t)]^{0.5} = A_p \frac{dZ}{dt}$$

where A_p is the cross-sectional area of the former plate. Integration of the above equation yields the following expression for the discharge time (t_d):

$$t_d = (2A_p/C_d A_f) \, [Z^{0.5}/(2g)^{0.5}] \quad .$$

An estimate of t_d is presented in Table 6, indicating a drainage time of approximately 13 s (assuming melt debris occupies the entire volume space between two stacked former plates and all holes in the former plate available for drainage). The implication of this result is that rapid drainage of melt debris through the series of eight former plates would have occurred, <u>if such debris remained in the molten state</u>. However, the fact that a significant amount of debris has been observed in the core-former volume space and that the reactor vessel is estimated to have been reflooded (except for the dryout region of consolidated core debris) by ECC injection after 200 min, implies resolidification of once-molten debris in the core-former region upon contact with coolant. In-place refreezing of debris when exposed to coolant in the core-former volume space is consistent with the observation of the presence of resolidified melt debris fused to or resting on the former plates.

TABLE 6. MELT DRAINAGE TIME THROUGH CORE-FORMER PLATE FLOW HOLES

Governing Equation

$t_d = (2A_p/C_dA_f)\ [Z^{0.5}/(2g)^{0.5}]$

Parameter Values

g = gravitation constant = 32.2 ft/s^2 = 980 cm/s^2

A_p = cross-sectional area of core-former plate[a] = 17.8 ft^2 - 16.54 E+3 cm^2

A_f = total flow area of holes in core-former plate (fifth level plate) = 71.92 in.^{2} = 464 cm^2

C_d = discharge coefficient = 0.9

Z = degris height = height between fifth and sixth core-former plates = 22 in. = 55.9 cm

$$\frac{2A_p}{C_dA_f} = \frac{2\ (16.54\ E{+}3\ cm^2)}{0.9\ (464\ cm^2)} = 79.2$$

$Z^{0.5}/(2g)^{0.5}$ = 0.1689 s

t_d = 79.2 x 0.1689 s = 13.4 s

a. D. W. Golden, "TMI-2 Standard Problem Package," EGG-TMI-7382, September 1986, pp. 4-24, Table 11.

In addition to an evaluation of debris migration behavior in the core-former region, an assessment is made of melt-debris/former-plate thermal interaction.

5.2 Debris/Former Plate Thermal Interaction

To assess the potential for corium melt attack on the former plates, the geometry illustrated in Figure 11 is employed, consisting of an overlayer of molten corium that conducts heat to the cooler core-former plate. For practical purposes, the core debris region can be considered a semi-infinite slab (region-1) at an initial bulk temperature (T_a), with a constant heat transfer coefficient (h) at the contact surface. The former plate (region-2) is of finite thickness, δ, and with an adiabatic surface at $x = \delta$. Each region has different material and heat conduction properties. Neglecting the decay-heat source term in region-1, the situation is similar to that assessed previously in Section 4.2.

The solution to transient heatup of the former plate can be expressed as functions of the dimensionless Fourier (Fo) and Biot (Bi) numbers. For conduction-controlled heat transfer, the Biot number reduces to the conductivity ratio, whereas F_o is the ratio of thermal penetration distance to the wall thickness, that is,

$$Bi = k_1/k_2$$

$$Fo = \alpha t/\delta^2 \quad .$$

Using the charts presented in Figures 12 and 13,[27] the temperature of the former plate can be obtained as a function of time (t) and distance (x).

Parameter values are estimated in Table 7 for former-plate heatup to the melting point of stainless steel (2500°F), at an initial debris temperature corresponding to that for UO_2 melting (4670°F) and 500°F superheat (5170°F):

$$Bi = k_1/k_2 = 0.22$$

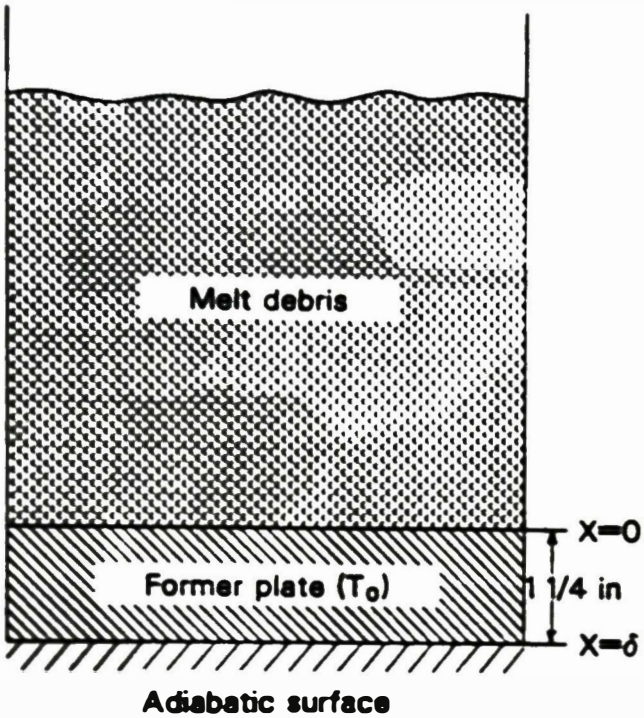

P445-LN87038-6

Figure 11. Illustration of semi-infinite melt debris in contact with core-former plate of finite thickness (δ), and nil heat transfer at lower surface (x = δ).

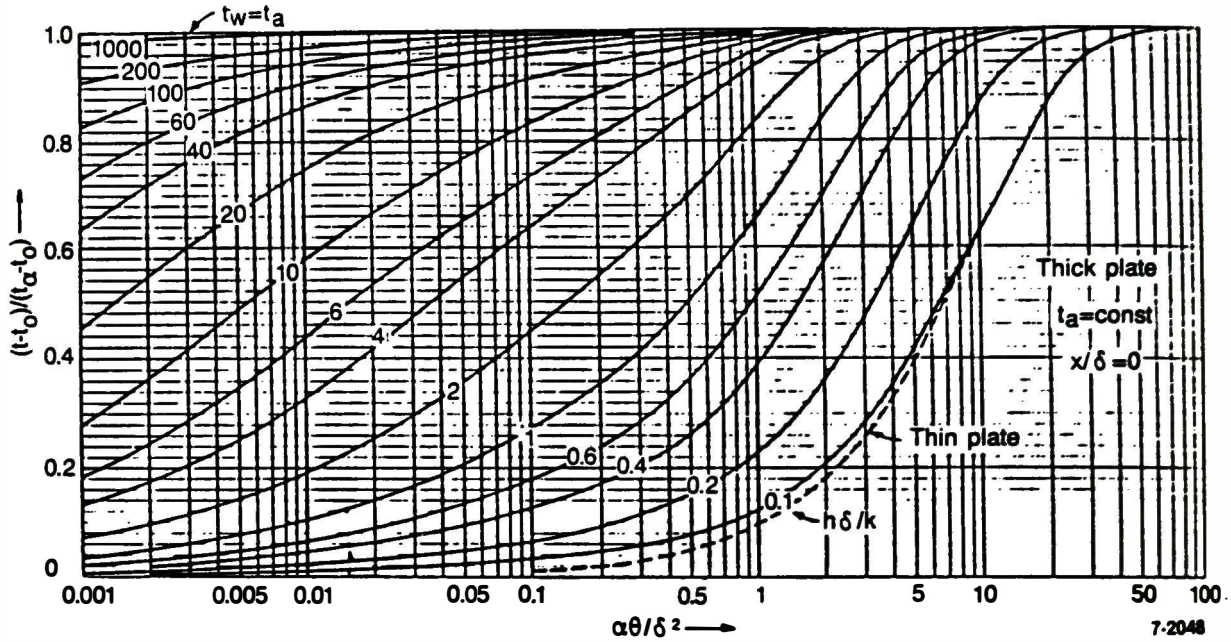

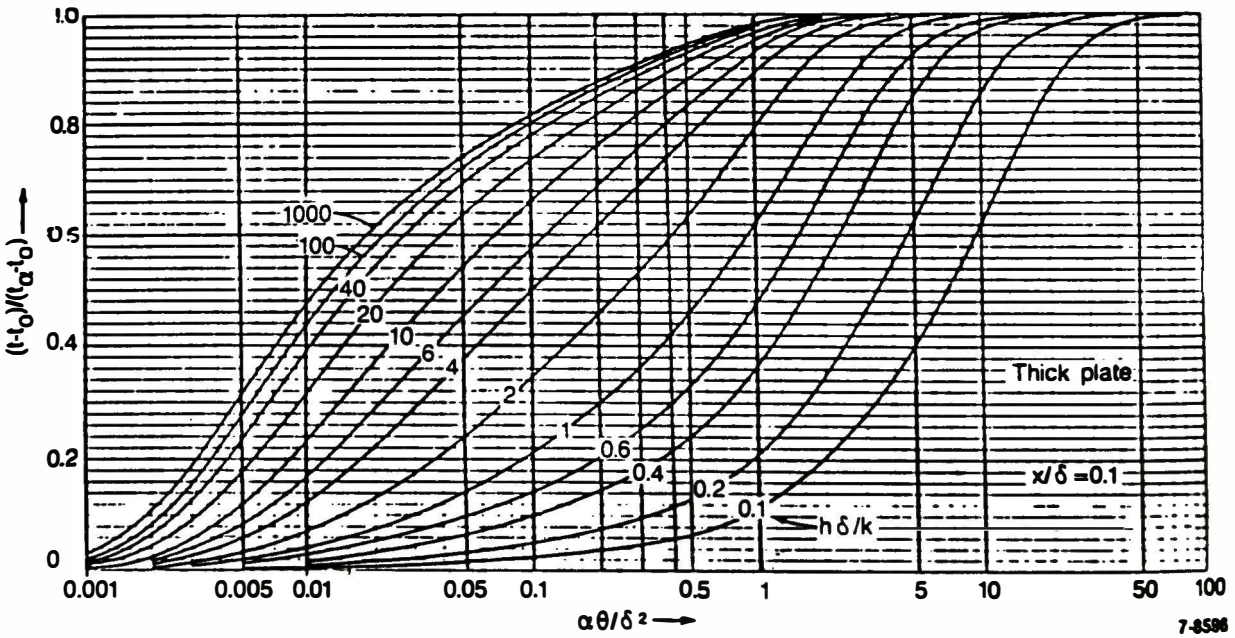

Figure 12. Temperature response of thick plate ($0 \leq x \leq \delta$), insulated at the surface ($x = \delta$) after sudden exposure to temperature; solution at T_a, $x/\delta = 0$ and $x/\delta = 0.1$.

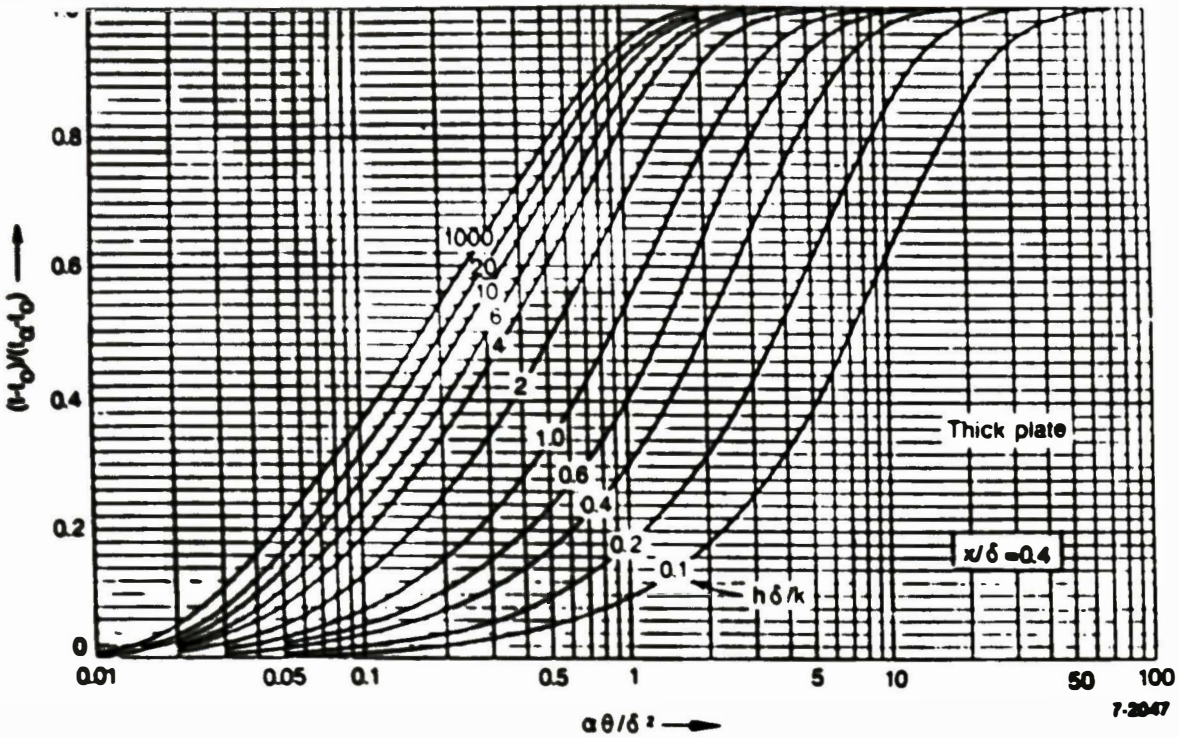

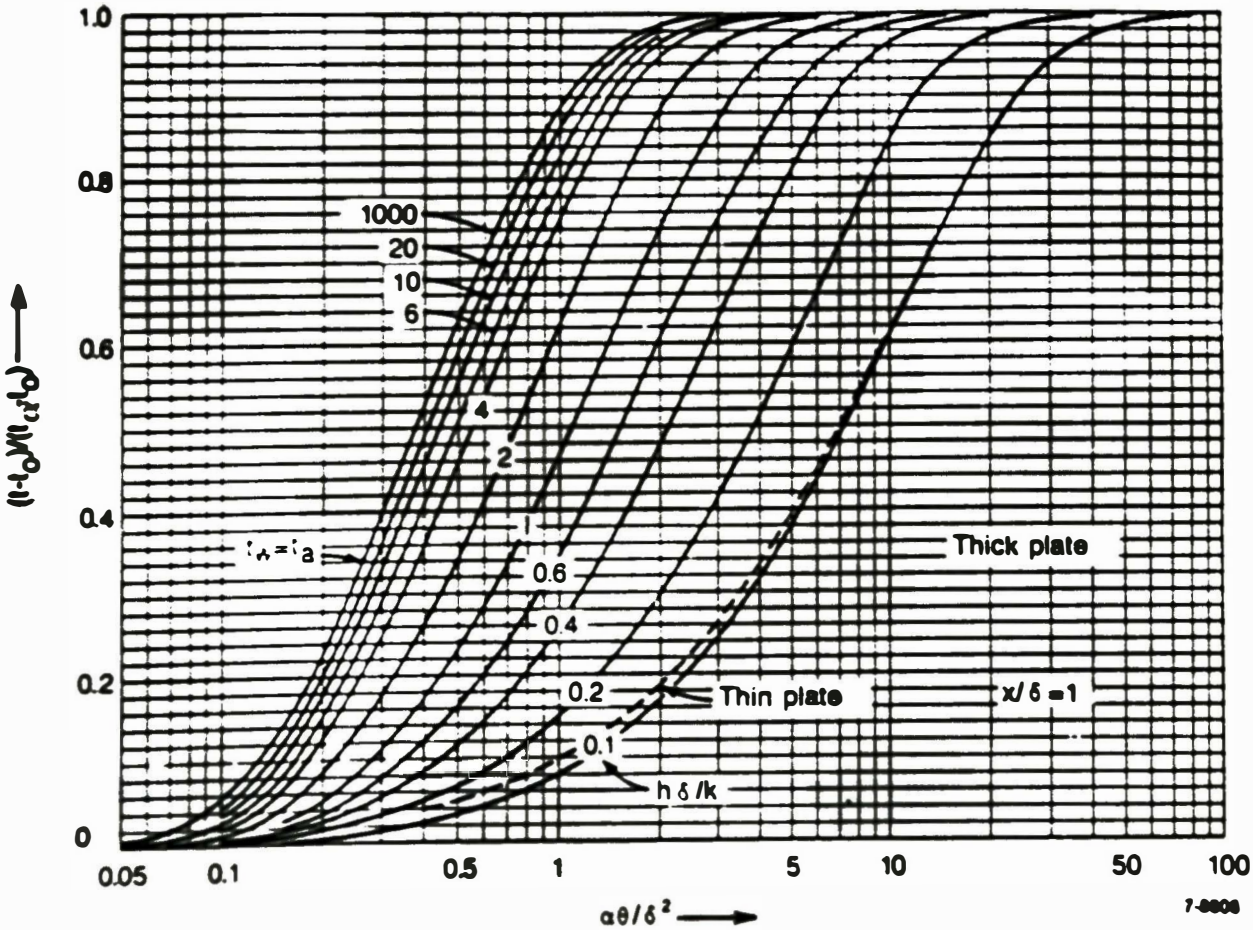

Figure 13. Temperature response of thick plate ($0 \leq x \leq \delta$), insulated at the surface ($x = \delta$), after sudden exposure to temperature, T_a, solution at $x/\delta = 0.4$ and $x/\delta = 1$.

TABLE 7. HEAT-TRANSFER PROPERTIES OF STAINLESS-STEEL FORMER PLATE IN CONTACT WITH UO_2 MELT DEBRIS

Thermophysical Properties of Former Plate (Stainless-Steel)

T_{mp} = 2500°F = 1640 K

C_p = 0.12 B/lb°F = 0.12 cal/g K

k = 9.4 8/h-ft-°F = 16.26 W/m-K

$\rho = 0.26 \frac{lb}{in.^3} = 500\ lb/ft^3 = 80\ kg/m^3$

$\alpha = k/\rho C_p = 9.4/500\ (0.12) = 0.157\ ft^2/hr = 0.0063\ in.^2/s$

L (Fe) = 65 cal/g = 117 B/lb

Thermophysical Properties of the UO_2 Melt Debris

T_{mp} = 4670°F = 2850 K

C_p = 0.12 B/lb-°F = 0.12 cal/g-K

K = 2.1 B/lb ft °F

$\delta_L = 8.7\ g/cm^3 = 543\ lb/ft^3$

$\alpha = k/\rho C_p = 0.032\ ft^2/hr$

L = 119 8/lb = 66 cal/g

Biot Number, Bi

$Bi = k_1/k_2 = 2.1/9.4 = 0.22$

Temperature Ratio, $T-T_o/T_a-T_o = T'$

T = melting point of stainless steel = 2500 °F

T_a = core debris melt temperature

T_o = initial temperature of baffle plate = water saturation temperature at 1500 psi ≈600 °F

$T-T_o/T_a-T_o = 2500-600/T_a-600$

TABLE 7. (continued)

<u>Case 1</u>

T_a = UO_2 melting point = 2850 K = 4670°F

T' = 0.47

<u>Case 2</u>

T_a = UO_2 melting point + 500°F superheat = 5170°F

T' = 0.42

$T' = 0.47$ (at UO_2 melting point)

$T' = 0.42$ (500°F UO_2 superheat).

Making use of Figure 13, the associated Fourier number at $x = \delta$ is estimated to be

$$Fo \text{ (at } T' = 0.42) = \alpha t/\delta^2 = 3.0$$

$$Fo \text{ (at } T' = 0.47) = \alpha t/\delta^2 = 3.5 \quad .$$

Thus, the time for complete melt-through of the 1-1/4-in.-(0.1042-ft)-thick former plate is estimated to be on the order of

$$t = 3.0\ \delta^2/\alpha = 3.0\ (0.1042\ ft)^2/(0.1567\ ft^2/hr) = 0.21\ hr$$

$$t = 3.5\ \delta^2/\alpha = 0.24\ hr$$

or approximately 12 to 15 min. As indicated in the previous section, (see Section 5.1.2), the time associated with melt drainage through the flow holes of two stacked/adjacent former plates is estimated to be approximately 13 s, which is much less than the time for melt-through of the former plate. Thus, little melt ablation of the former plate is indicated.

5.3 Discussion

Although questions remain as to the presence of core debris in the former region and attendant thermal interaction potential, from the preceding analysis the following scenario is postulated relative to molten corium migration and melt ablation processes in the core-former region.

Based upon a comparison of available flow areas, it appears that the flow holes of the former plates offered insufficient flow area to accommodate melt relocation through the available flow area of the melt-ablated east-quadrant baffle plates. The implication of this

comparison is that partial lateral migration of melt debris along the surface of the core-former plates occurred. Such lateral migration of molten corium is consistent with the general pattern of the debris configuration data illustrated in Figure 7, that is, maximum debris presence at the east-quadrant location where baffle plate melt-through has been observed, with a diminishing debris depth at increasing circumferential orientations away from the east-quadrant baffle-plate melt-through holes.

The potential for melt ablation of the former plates was assessed from consideration of former-plate thermal response to direct contact with molten corium. Assuming perfect contact and conduction-controlled heat transfer, the time for melt-through of the 1-1/4-in.-thick stainless-steel former plate was estimated to be approximately 15 min in a dry environment. The presence of water in the former plate volume space would appreciably extend the time for melt ablation of the former plates. Since the drainage time for direct melt migration through the former-plate flow holes (80 holes per plate) was estimated to be 13 s, little melt ablation of the former plates is inferred. Likewise, since the time period over which the major debris migration event occurred (at 225 min) is estimated to be about 1-2 min, little melt ablation of the former plates is also inferred over this time period. Thus, it can be surmised that notable melt ablation of the core-former plates is not expected.

Since reactor vessel reflooding (at ≈200 min.) is estimated to have occurred before the corium melt relocation event at about 225 min, the presence of debris (≈13,600 lb) in the core-former volume space is thought to be due to quenching/refreezing of molten corium upon entry into the core-former volume space. Quenching of melt debris into refrozen/agglomerated particles is considered the likely cause for debris retention on the core-former plates. The former plates are assessed to have remained intact; however, core debris may be fused to the former plates as a consequence of debris quenching/refreezing in this region.

6. DEBRIS THERMAL ATTACK ON THE LOWER HEAD

In addition to an assessment of corium melt attack on the core former assembly, relocation of corium melt to the lower plenum poses questions concerning thermal interaction of melt debris with the lower head. Previous analysis[15] of the lower head indicates that the stainless-steel liner is not likely to have experienced melting upon contact with either metallic- or ceramic-like melt debris. The geometry considered in that analysis was one of a melt pool spread uniformly over the head surface. However, the recent update of the melt-relocation scenario indicates that the major fraction of core relocation most likely occurred in the east quadrant of the vessel, where drainage may have occurred in the form of a coherent jet. The question then arises as to whether an impinging jet of molten corium could have resulted in localized melt ablation of the head. This question is investigated here. The first parameter to be estimated is the time period (t_j) over which melt debris drainage in the form of a jet can be expected. Lower head heatup is then assessed for various assumptions regarding jet characteristics and debris/head thermal interaction.

6.1 Jet Drainage Time

To assess a characteristic drainage time, the geometry illustrated in Figure 14 is employed, where it is assumed that a volume of melt debris (V_m) relocates as a coherent jet with a cross-sectional area (A_j). Assuming gravity-controlled drainage and a jet discharge velocity (V_j) that is significantly larger than that of the free interface (V_2) at Z_2, the well-known Bernoulli equation for the discharge or jet velocity (V_j) can be used, that is,

$$V_j = C_d \, [2g \, (Z_2 - Z_1)]^{0.5}$$

where C_d is a discharge coefficient (for smooth openings, a value of ≈0.9 can normally be assumed).

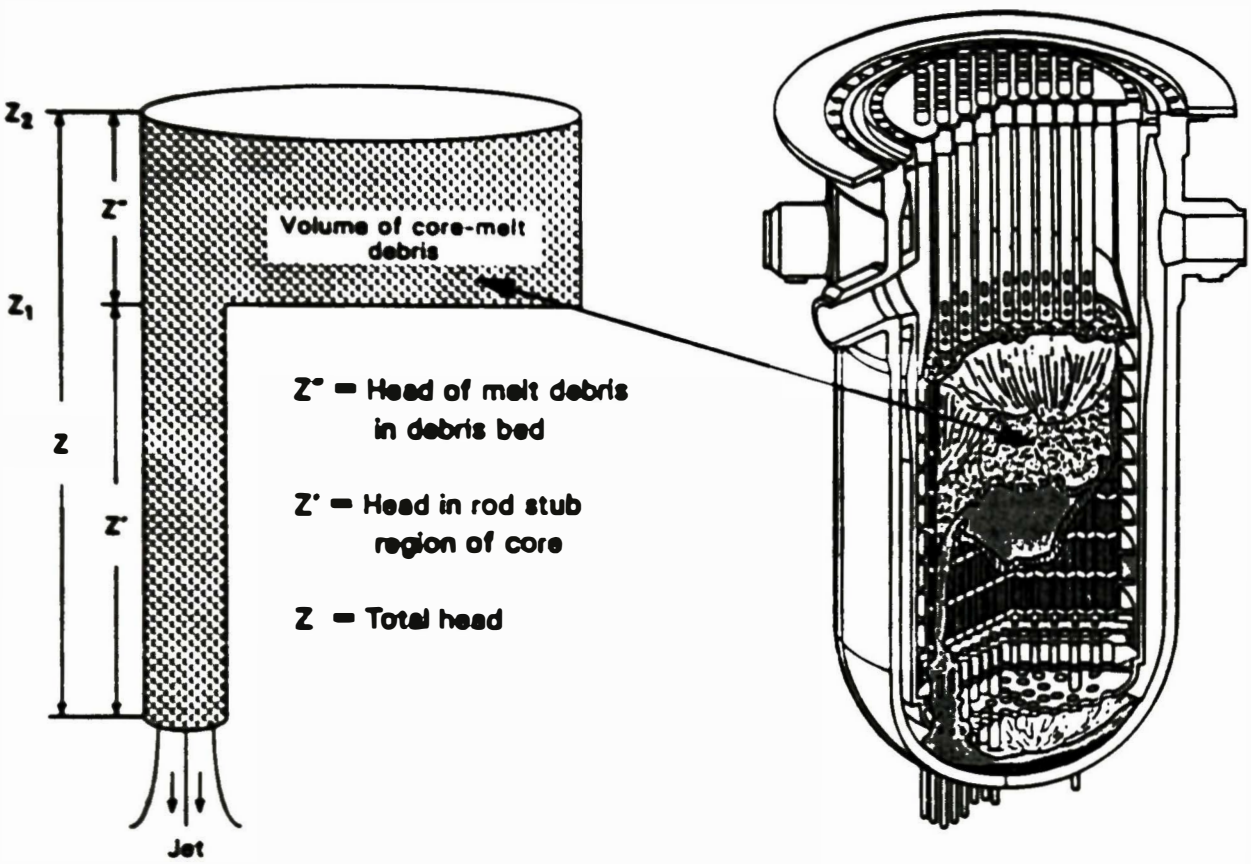

Figure 14. Illustration of core melt configuration for assessment of melt drainage time.

Applying the continuity equation, where the mass outflow of the jet is equated to the mass loss from the pool, the jet velocity (V_j) can be expressed in terms of the geometric properties of the melt pool:

$$A_j V_j = A_j C_d [2gZ(t)]^{0.5} = A_p \frac{dZ(t)}{dt}$$

where

A_j = jet cross-sectional flow area

A_p = pool cross-sectional flow area

$Z(t)$ = height of melt pool.

Integration of the above equation yields the following expression for the melt drainage or jet impingement time (t_j):

$$t_j = \frac{2}{C_d} \left(\frac{A_p}{A_j}\right) \left(\frac{Z''}{2g}\right)^{0.5}$$

where Z'' equals the initial pool height.

As indicated, t_j depends upon the dimensional characteristics of the melt pool and the jet size. Since the active fueled region of the core has an equivalent diameter of approximately 10.7 ft (Reference 26), and since the molten pool is considered to have extended to all but peripheral fuel assemblies, the equivalent pool diameter (D_p) is assumed to be on the order of approximately 9 ft, with an associated cross-sectional area of about 64 ft^2 (5.95 m^2). Noting that the amount of prior molten debris in the lower plenum is estimated to be on the order of 20 metric tons (20,000 kg; Reference 27) and assuming a corium melt density of 8 g/cm^3, the associated initial pool height (Z") is estimated to be

$$Vol_p = \frac{20\ E{+}6\ g}{8 g/cm^3} = 2.5\ E{+}6\ cm^3 = 2.5\ m^3$$

$$Z'' = 2.5\ m^3/5.95\ m^2 = 0.42\ m\ (1.38\ ft) \quad .$$

Based on evidence[4,5] that the major portion of melt relocation occurred in the east quadrant and within several fuel assemblies (one-to five assumed here, where the nominal area for coolant flow through an undegraded fuel bundle is on the order of 39.6 in.^{2} or 0.275 ft^2), the jet cross-sectional flow area (A_j) is estimated to be

$$A_j = 0.275\text{-}1.375\ ft^2\ (0.0255\text{-}0.128\ m^2) \quad .$$

Using the above estimated parameters, with $C_d = 0.9$ and $g = 32.2\ ft/s^2$, the jet discharge time (assuming 1 to 5 open fuel assemblies for melt drainage) is estimated to be

$$t_j\ (A_j = 1\ \text{assembly}) = \frac{2}{0.9}\left(\frac{64}{0.275}\right)\left(\frac{1.38}{64.4}\right)^{0.5} = 75\ s$$

$$t_j\ (A_j = 3\ \text{assemblies}) = 25\ s$$

$$t_j\ (A_j = 5\ \text{assemblies}) = 15\ s \quad .$$

Thus, the jet discharge time ranges from about 75 s assuming drainage through one fuel assembly, to about 15 s for drainage through five fuel assemblies. This compares favorably with the 1-to-2-min melt relocation time estimated in Reference 7, from SPND and other TMI-2 data (see Section 2).

As illustrated in Figure 15, the lower plenum contains several structures through which the melt-debris jet must penetrate before it impacts the lower head. For our present purposes, coherent jet penetration is assumed up to the flow distributor forging. Noting that the distributor forging has flow holes 6 in. in diameter, the jet flow area in the lower plenum is taken to be

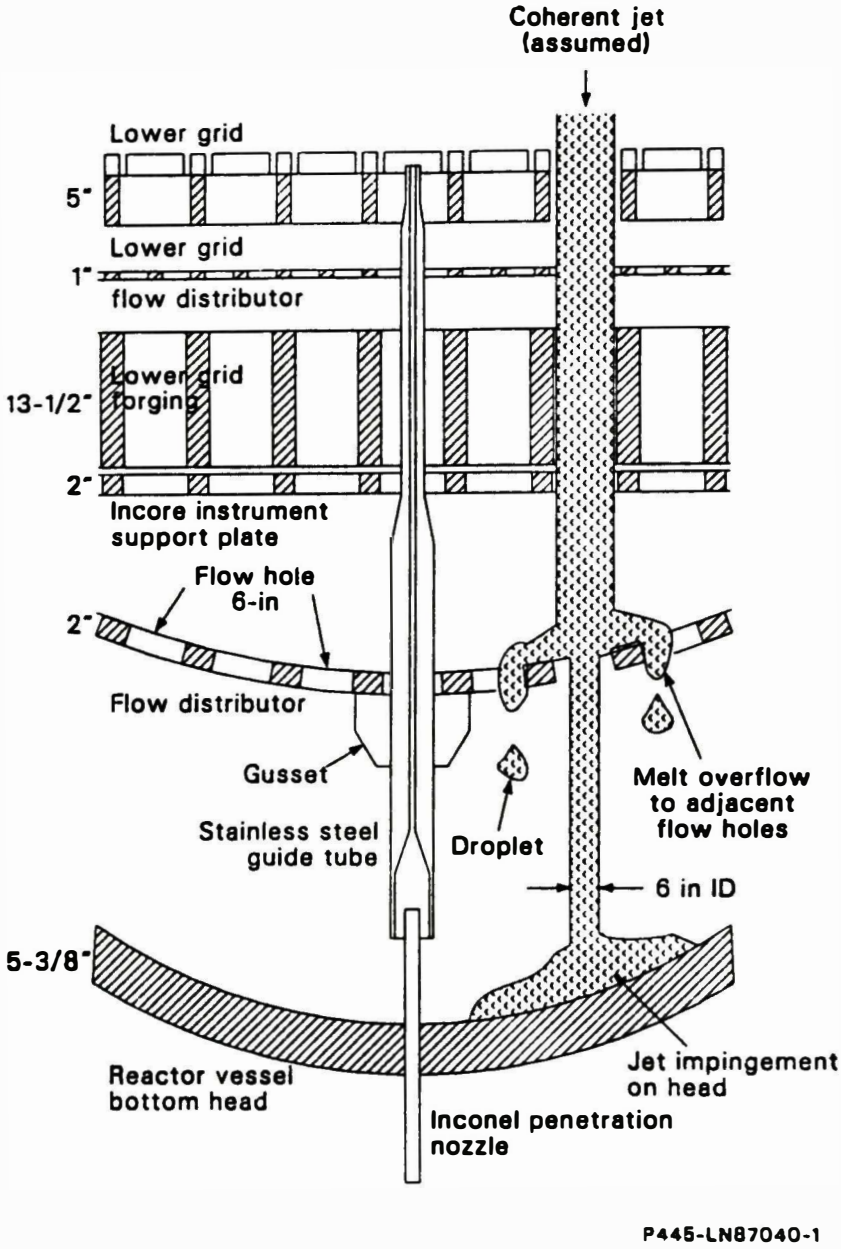

Figure 15. Illustration of TMI-2 lower plenum structures and assumed melt-penetration/jet-impingement geometry.

$$A_j = 0.25\ \pi\ (6\ \text{in.})^2 = 28.3\ \text{in.}^2\ (0.196\ \text{ft}^2) = 0.018\ \text{m}^2 \quad .$$

Since the flow area of a distributor hole is less than that of a single fuel assembly, some overflow at the distributor plate can be expected. For our present purposes, jet impingement characteristics are defined by the core discharge time (t_j) associated with a single fuel assembly and the flow area (A_d) of a single distributor hole, that is,

$$t_j = 75\ \text{s}$$

$$A_j = 0.018\ \text{m}^2 \quad .$$

Localized lower head heatup for such jet impingement characteristics is assessed next.

6.2 Lower Head Heatup by Jet Impingement

To assess heatup of the lower head by direct jet impingement, an estimate is made of the contact temperature at the jet/head interface. The temperature profile in the head for a 75 s contact period is also assessed for various assumed thermal conditions of the jet.

6.2.1 Initial Contact Temperature

The configuration of jet debris contact with the lower head is shown in Figure 16. To determine if initial melting of the stainless steel liner on the inside surface of the reactor vessel will occur, the following conduction-limited relationship for the instantaneous contact interface temperature for two semi-infinite slabs can be employed, that is,

$$T_I = \frac{T_H\ (k/\alpha^{0.5})_H + T_C\ (k/\alpha^{0.5})_C}{(k/\alpha^{0.5})_H + (k/\alpha^{0.5})_C}$$

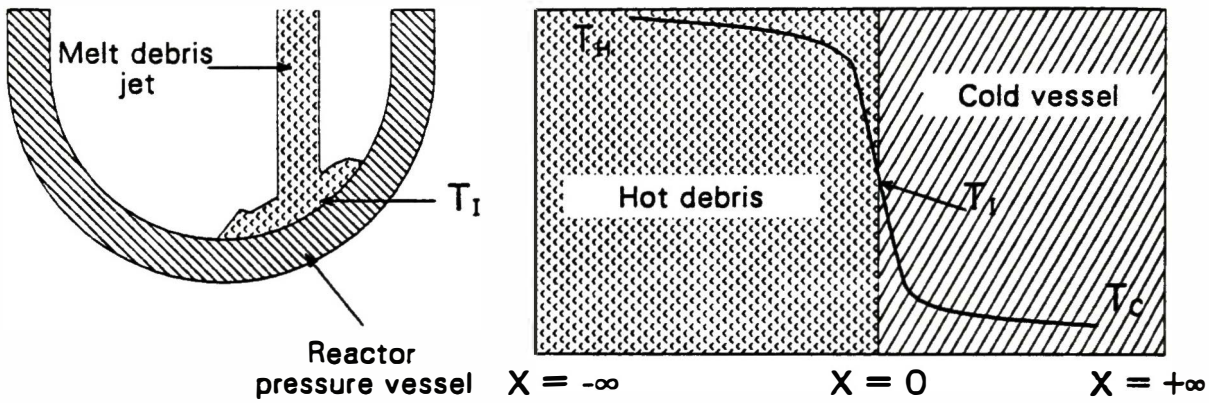

P445-LN87040-3

Figure 16. Illustration of bottom-head thermal attack by corium melt.

where

T = temperature

k = thermal conductivity

α = thermal diffusivity

H = hot material debris

C = cold material (reactor vessel).

The configuration illustrated in Figure 16 is essentially the same as that previously assessed in Section 4-1, where the bulk temperature of the head (T_C) is taken as the saturation temperature of water corresponding to a pressure of 1500 psi (T_C = 596°F = 586 K). Calculational results presented in Section 4 (see Table 3), assuming UO_2 debris thermal properties, indicate that because of the higher conductivity of the vessel wall compared to the ceramic-like debris, the interface temperature is closer to the bulk temperature of the vessel rather than of the debris. Since the melting points of the stainless-steel liner and carbon steel are 2500°F and 2750°F, respectively, melting of either material is not predicted for contact with ceramic UO_2 debris at debris temperature as high as 7000°F (4144 K).

Table 4 presents a similar calculation; however, the melt debris is considered to be a mixture of U-Zr-O components, with an effective metal-like conductivity of 50 W/m-K (28.9 B/h-ft-°F). This increase in debris thermal conductivity results in an interface temperature that partitions the bulk debris and vessel wall temperatures. Thus, inside surface melting upon initial contact may occur for metallic-like debris if its melt temperature exceeds ≈4500°F (2755 K). However, such a high melting point is more typical of a ceramic-like debris.

It should be noted that the instantaneous contact temperature is based upon contact between two semi-infinite materials of different thermal

conductivities and bulk temperatures. As such, the solution is valid only for conduction-controlled heat transfer prior to thermal front penetration through the thickness of either material. Thus, the above estimate is simply an indication of the initial contact temperature of the inside surface of the vessel head upon initial jet impingement. The implication is that surface melting of the stainless-steel liner is not likely on initial contact with ceramic debris properties, and only for metallic debris well above (>2750 K) the α-Zr(O)/UO_2 eutectic temperature ($\simeq$2170 K). Since initial liner melting is not predicted, the question then centers on potential heatup of the lower head during the time period (t_j) of melt drainage and jet impingement.

Various heat-transfer and jet-impingement conditions can be postulated that largely impact predicted behavior. For weak jets, the primary mode of heat transfer is considered to be conduction. However, turbulent mixing and mass transfer effects in strong jets could lead to an enhanced convection-controlled heat transfer process, where hot melt debris is always in contact with the vessel head. These two limiting conditions are assessed. For present purposes, it is also assumed that the jet is of sufficient strength, that any crust is unstable, and direct jet contact with the head occurs. For these assumed conditions, both convection- and conduction-controlled heat transfer are investigated at the jet/head interface.

6.2.2 Conduction-Controlled Transient Heatup of the Lower Head

Figure 17 illustrates the essential features of the problem, where the lower head is represented by a wall of finite thickness in local contact with a jet of infinite length. Assuming one-dimensional heat transfer in the x-direction, the problem can be approximated as a semi-infinite material (region-1) in contact with a material of different conduction properties (region-2), which is of finite thickness (δ) and insulated at the surface $x = \delta$. Neglecting the decay-heat source term in region-1, the situation is similar to that assessed previously in Section 5.

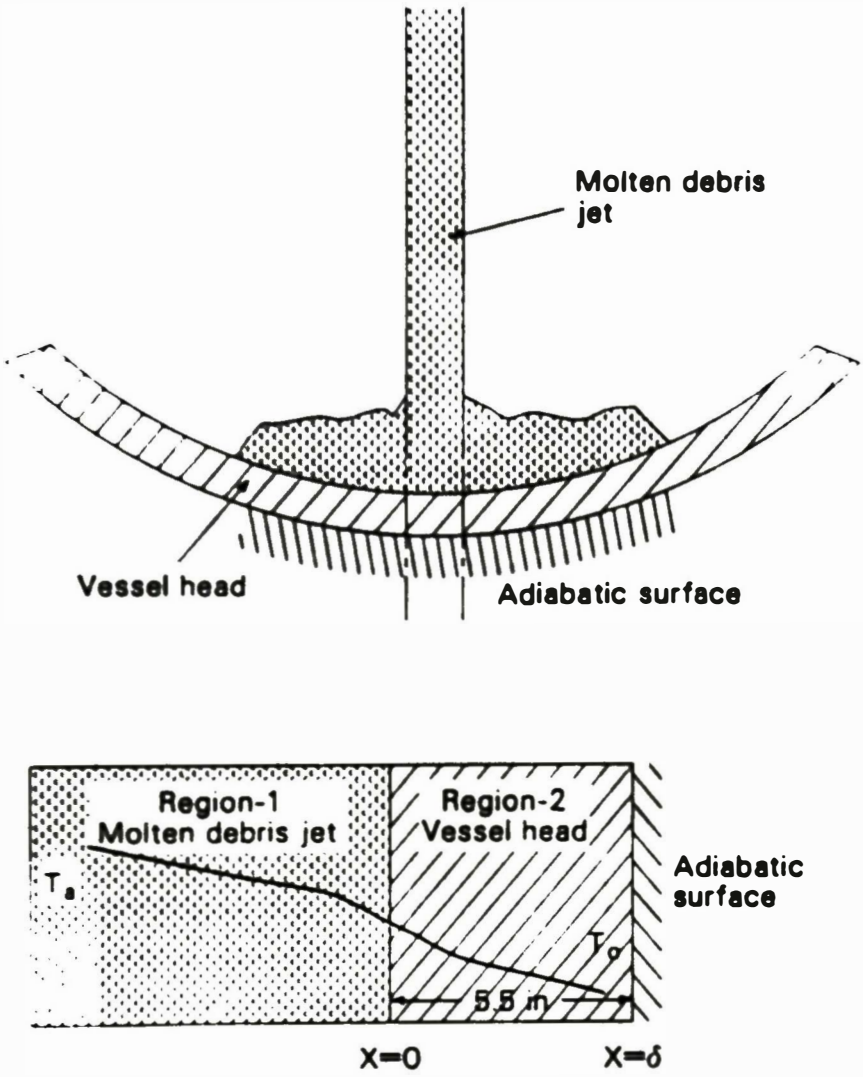

Figure 17. Illustration of jet/vessel head thermal conduction problem, assuming contact of a semi-finite region of hot melt with a conducting material of finite thickness (δ) insulated at the surface x = δ.

The solution can be expressed as functions of the dimensionless Fourier (Fo) and Biot (Bi) numbers. For <u>conduction-controlled heat transfer</u>, the Biot number reduces to the conductivity ratio, while F_o is the ratio of thermal penetration distance to the wall thickness, that is,

$$Bi = k_1/k_2$$

$$Fo = \alpha t/\delta^2 \quad .$$

Using the charts presented in Section 5 (see Figures 12 and 13), the temperature in the lower head as a function of time (t) and distance (x) can be obtained. The time period of interest is the melt drainage time associated with jet impingement (t_j = 75 s). Parameter values of the dimensionless groups are estimated in Table 8 for UO_2/stainless-steel contact:

$$Bi = 0.22$$

$$Fo \text{ (at } t_j = 75 \text{ s)} = 0.0156 \quad .$$

As indicated relatively low temperatures are maintained in the lower head over the 75-s time period estimated for jet impingement. Such low head temperatures are caused by the rather small Biot number, where the low conductance of the jet material (assumed to have UO_2 ceramic-like properties) controls the heat transfer process.

To assess the time period for surface (x/δ = 0.0) melting of the 5.5-in.-thick lower head, the Fo number is estimated from Figure 12 for the following dimensionless Bi and T' numbers (at a stainless-steel melting point of 2500°F):

$$T' = \frac{2500-600}{4670-600} = 0.467$$

TABLE 8. ESTIMATED TEMPERATURE RESPONSE OF THE LOWER HEAD CAUSED BY JET IMPINGEMENT (t_J = 75 s)

Thermophysical Properties of Vessel Head (Region-2)

T_{mp} = 2500°F = 1640 K

C_p = 0.12 B/lb°F = 0.12 cal/g K

k = 9.4 B/h-ft-°F = 16.26 W/m-K

$\rho = 0.26 \frac{lb}{in.^3} = 500\ lb/ft^3 = 80\ kg/m^3$

$\alpha = k/\rho C_p = 9.4/500\ (0.12) = 0.157\ ft^2/h$

L (Fe) = 65 cal/g = 117 B/lb

δ = head thickness ≈5.5 in. = 0.458 ft = 3.97 m

Biot Number, Bi

k_1 (UO_2) = 3.66 W/m-K

k_2 (steel) = 16.26 W/m-K

$Bi = k_1/k_2 = 3.66/16.26 = 0.22$

Fourier Number, Fo

$Fo = \alpha t/\delta^2$

$\alpha = 0.157\ ft^2/h$

t = 75 s = 0.0208 h

δ = 0.458 ft

$Fo = 0.157\ (0.0208)/(0.458)^2 = 0.0156$

Temperature Ratio, $T-T_o/T_a-T_o = T'$

T = lower heat temperature at x

T_a = core debris temperature = UO_2 melting point = 2850 K = 4670°F

T_o = initial temperature of baffle plate = water saturation temperature at 1500 psi ≈600 °F

$T' = \frac{T-600}{4670-600} = \frac{T-600}{4070}$

TABLE 8. (continued)

Solution From Charts

x/δ	x	T' (charts)	T (at x), °F
0.0	0.0	0.04	763
0.1	0.0458 ft (0.55 in.)	0.03	722
0.4	0.1832 ft (2.2 in.)	0.0	600
1.0	0.485 ft (5.5 in.)	0.0	600

$Bi = 0.22$

$Fo = 3.0$ (Figure 12) $= \alpha t/\delta^2$

$t = 3.0\ (0.458\ ft)^2/0.157\ ft^2/hr = 4.0\ hr$.

As indicated, for ceramic-like debris, approximately 4 hr of contact are required before surface melting is predicted. This relatively long time is due to the combined effects of the relatively high heat capacity of the 5.5-in.-thick head, its relatively low initial temperature (≈600°F), and its high thermal conductivity compared to that of the corium heat source. Although decay-heat and phase-transformation effects have been neglected in the present analysis, such analysis illustrates the relatively high thermal capacity of the head when subject to thermal attack by low-conductivity ceramic-like debris. A simple check of such results can be accomplished by estimating the thermal relaxation time of the 5.5-in.-thick vessel head, that is,

$t = 2\delta^2/\alpha = 2(0.458\ ft)^2/0.157\ ft/hr = 2.67\ hr$.

Thus, almost 3 hr are required for thermal front penetration through the vessel, with an additional hour required to heat the surface to its melting point.

The situation is also investigated for a metallic-like jet. Assuming equivalent thermal conductivities in both the jet and head, the Biot number becomes unity, while the Fo at $t_j = 75$ s remains the same, that is, $Fo = 0.0156$. For the same initial debris temperature (that is, the UO_2 melting point of 4670°F), and a corresponding dimensionless temperature ($T' = T-600/4070$), the wall temperature at various distances (x) within the vessel head, at an exposure time of 75 s, can be estimated from Figures 12 and 13, that is,

x/δ	x	T' (charts)	T (at x)
0.0	0.0	0.12	1088
0.1	0.0458 ft (0.55 in.)	0.06	844
0.4	0.1832 ft (2.2 in.)	0.0	600
1.0	0.485 ft (5.5 in.)	0.0	600

A comparison with results presented previously in Table 8 for a ceramic-like jet material indicates that the high-conductivity metallic-like debris results in somewhat higher head temperatures. Nevertheless, for the 75-s time period of jet impingement, the vessel head is assessed to remain well below the melting point of the stainless-steel liner (T_{mp} = 2500°F). Thus, whether the jet has ceramic or metallic thermal properties, for conduction-controlled heat transfer surface ablation of the lower head by jet impingement is not indicated. Consideration of decay-heat and phase-transformation effects would not alter this conclusion.

6.2.3 Convection-Controlled Transient Heatup of the Lower Head

The analysis presented in the previous section was based upon the assumption of conduction-controlled heat transfer, where the Biot number reduces to the conductivity ratio. However, enhanced heat transfer above that caused by conduction can occur if significant turbulence at the jet head occurs. This situation is investigated here, where an effective heat transfer coefficient (h) is sought. For direct jet impingement on a flat plate, the following correlation has been suggested[28,29] for the Nusselt number (Nu) and heat transfer coefficient (h) at the plane of contact between the jet and wall:

$$Nu_j = 0.55\ Pr^{0.35}\ Re^{0.5}$$

$$\frac{hD}{k} = 0.55 \left(\frac{C_p \mu}{k}\right)^{0.35} \left(\frac{DV\rho}{\mu}\right)^{0.5}$$

where Pr = Prandtl number, Re = Reynolds number, D = jet diameter, V = jet velocity, ρ = density, μ = viscosity, C_p = specific heat, and k = thermal conductivity. All but D and V are known physical properties depending on the jet material. As discussed previously, the jet diameter (D) is assumed equal to the 6-in. (0.5-ft) diameter flow hole of the distributor, whereas the jet velocity (V_j) is defined by the differential height (ΔH) between the flow distributor forging and the lower head (≈3 ft), that is,

$$V_j = (2g\Delta H)^{0.5} = [2(32.2\ ft/s^2)(3\ ft)]^{0.5} = 13.9\ ft/s\ (\approx 50{,}000\ ft/hr) \quad .$$

The associated heat transfer coefficient (h), Biot number, and temperature distribution in the vessel head are given in Table 9. As indicated, the <u>surface temperature</u> of the head for convection-controlled heat transfer is estimated to be approximately 4500°F (2755 K). This surface temperature is significantly greater than that predicted for solely conduction-controlled heat transfer in the debris jet (see Table 8), and is greater than the liner melting point (≈2500°F). Thus, for jet turbulence, surface melt ablation of the stainless-steel liner is indicated. However, the depth of penetration of the melt front in the vessel head is estimated to be only on the order of x/δ = 0.1 at t = 75 s (that is, 0.55 in. versus a head thickness of 5.5 in.). Thus, limited loss of vessel structured integrity is expected for a jet impingement time on the order of 75 s.

An estimate of the time for the vessel head 1/2-thickness to reach melting can also be assessed from the charts presented in Figure 12. For x/δ = 0.4, Bi = 100, T_{mp} = 2500F, and T' equals

$$T' = \frac{2500-600}{4670-600} = 0.47 \quad .$$

A Fourier number of 0.17 is estimated from Figure 12. Thus, the associated time for melt penetration to a head thickness of x/δ = 0.4 (2.2 in.) is

TABLE 9. JET HEAT TRANSFER COEFFICIENT AND TEMPERATURE RESPONSE OF THE LOWER HEAD CAUSED BY JET IMPINGEMENT (t_J = 75 s)

Jet Thermophysical Properties (UO_2)

T_{mp} = 2500°F = 1640 K

C_p = 0.12 B/lb°F = 0.12 cal/g K

k = 3.66 W/m-K = 2.1 B/hr-ft-°F

ρ_L = 8.7 g/cm^3 = 543 lb/ft^3 = 8.69 g/cm^3

μ(molten UO_2) = 4(10^{-2}) g/cm-s = 9.68 lb/ft-hr

Dimensionless Parameters

Pr = $C_p\mu/k$ = 0.12 (9.68)/2.1 = 0.553

Re = $DV\rho/\mu$ = 0.5(50,000)(543)/9.68 = 14.0E+5

Jet Heat Transfer Coefficient

Nu = hD/k = .55 $(Pr)^{0.35}$ $(Re)^{0.5}$ = 0.55 (0.813)(1183) = 529

h = 529(2.1 B/hr ft °F)/(0.5 ft) = 2220 B/hr ft^2 F

Biot Number, Bi

Bi = $h\delta/k$

δ(vessel head) = 0.458 ft

k(vessel head) = 9.4 B/hr-ft-°F

Bi = 2220 (0.458)/9.4 = 108

Fourier Number, Fo

Fo (see Table 8) = 0.0156

Temperature Ratio, $T-T_o/T_a-T_o = T'$

T = lower heat temperature at x

T_a = core debris temperature = UO_2 melting point = 2850 K = 4670°F

T_o = initial temperature of baffle plate = water saturation temperature at 1500 psi ≈600 °F

$$T' = \frac{T-600}{4670-600} = \frac{T-600}{4070}$$

TABLE 9. (continued)

Solution From Charts

x/δ	x	T' (charts)	T (at x), °F
0.0	0.0	0.96	4500
0.1	0.0458 ft (0.55 in.)	0.54	2800
0.4	0.1832 ft (2.2 in.)	0.02	680
1.0	0.485 ft (5.5 in.)	0.0	600

$$Fo = 0.17 = \alpha t/\delta^2$$

$$t = 0.17\ (0.458\ ft)^2/0.157\ ft^2/hr = 0.23\ hr\ (14\ min)\ .$$

For direct jet impingement of 15-20 min, melt ablation of about half the vessel head thickness is concluded. With this event, loss of structural integrity of the vessel head would be expected.

6.3 Discussion

For the condition of sudden melt debris relocation, the situation can be envisioned where melt debris may relocate to the lower plenum in the form of a coherent jet and begin to thermally attack the steel vessel in this locale. Heatup of the lower head is largely dictated by the time over which jet impingement can be expected and the heat transfer characteristics at the impingement surface.

The jet drainage time (t_j) was assessed from consideration of the mass of core material (20,000 kg) estimated to have relocated to the lower plenum, and findings from various core examination efforts indicating east-quadrant relocation through several peripheral fuel assemblies (1-5 assumed in this analysis). For gravity-governed flow, the estimated drainage time was found to range from 75 s (1-fuel-assembly flow area) to 15 s (5-fuel-assembly flow area). Based on source range monitor response, indicating major relocation in the period of 1 to 2 min, a jet drainage time of 75 s was used in subsequent heatup analyses of the lower head.

Various jet-impingement heat-transfer characteristics can be postulated, which largely govern inferred lower head heatup behavior. Two limiting conditions were assessed. The first is for weak jet forces with conduction limited heat transfer. The second is for strong jet forces, where turbulent mixing and mass transfer effects lead to an enhanced convective-controlled heat transfer process.

For <u>conduction-controlled</u> heat transfer, surface ablation of the lower head by jet impingement is not predicted. For <u>convection-controlled</u> heat

transfer the following correlation was used to assess the effective heat transfer coefficient (h) at the plane of contact between the jet and lower head:

$$Nu_j = \frac{hD}{k} = 0.55\ Pr^{0.35}\ R_e^{0.5}$$

Calculational results indicate that the surface temperature is much greater than predicted for conduction-controlled heat transfer. For jet turbulence, <u>surface</u> melt ablation of the liner is predicted. However, the predicted depth of penetration of the melt front in the vessel head is on the order of about 0.5 in. (versus a head thickness of 5.5 in.), at a jet impingement time of 75 s. Thus, limited loss of vessel structural integrity is expected for jet impingement time on the order of 75 s. A direct jet impingement time of about 15-20 min is estimated for melt ablation of the vessel head 1/2-thickness, at which point head integrity cannot be assured.

7. SUMMARY AND CONCLUSIONS

Recent TMI-2 vessel inspection and core damage characterization efforts have provided a basis for an improved understanding of the TMI-2 accident scenario and damage progression. However, specific questions arise as to the nature and extent of core-melt interaction with vessel structural components. For example, questions remain as to why certain structures experienced significant melt ablation (e.g., lower plenum stainless-steel guide tubes, Inconel penetration nozzles, 3/4-in.-thick baffle plates), while other structures (lower core support forging, flow distributor plate) appear to have suffered little damage. This report presents analyses aimed at furthering the understanding of melt-debris/core-structure interaction, specifically the thermal response behavior of the vertical baffle plates, the horizontal core-former plates, and lower vessel head to thermal attack by molten corium.

7.1 Baffle Plates

Defueling efforts have resulted in removal of most peripheral fuel assemblies, as well as the rubblized debris that occupied the upper third of the original core. Subsequent video inspection of the vertical baffle plates shrouding the core periphery has revealed several large openings (8- to 9-in. long and about 3-in. wide) in these 3/4-in.-thick stainless-steel plates. The holes appear to have been caused by melt ablation. To advance the understanding of such baffle plate melt-through, an assessment was made of the contact time necessary for melt failure of the baffle walls.

The time for baffle-plate melt-through was assessed on the basis of conduction-controlled heat transfer, for the assumed geometry of semi-infinite molten debris in contact with a steel slab of finite thickness. Complete melt-through of the baffle wall thickness was calculated to occur in about 10 to 15 min. Since the axial location of east-quadrant baffle melt holes (≈4.75-ft elevation) is somewhat lower than the initial elevation of the uncoolable debris bed (≈8-9-ft elevation), and since the major melt relocation event at 225 min is thought

to have lasted only for about 1 to 2 min, baffle plate melt-through may not have been directly tied to events at 225 min. It can be postulated that holdup of a portion of the relocating debris during downward relocation, for a period of 10 to 15 min in the region of the baffle melt holes, could have been responsible for melt ablation of the baffle plates. However, partial melt debris drainage to lower elevations earlier in the accident, with a localized uncoolable blockage configuration, could also have been responsible for baffle melt failure at the 4.75-ft elevation. An examination of fuel assemblies, melt debris, and the baffle plate itself in the region of the melt holes (4.75 ft) is recommended to assess the nature of baffle plate failure and its relation to the overall TMI-2 melt progression scenario.

Since melt failure of the baffle plate will lead to potential melt relocation through the volume space between the baffle and core barrel, melt debris attack on the horizontal core-former plates was also investigated.

7.2 Former Plates

Fiberscope insertion data indicate that a significant amount of core debris is present on the horizontal core-former plates. Video inspection of the debris, as seen through the east-quadrant baffle plate melt-through holes, indicates once-molten debris characteristics.[25] Estimates indicate that upward of 6000 kg of once-molten corium resolidified in the core former volume space, with the highest blockage at the east side of the reactor. An assessment was therefore made of the migration behavior of melt debris during relocation through the core-former volume space and the potential for melt ablation of these 1-1/4-in.-thick stainless-steel former plates.

The volume space between the baffle plates and the core barrel is occupied by a series of eight 1-1/4-in.-thick stainless-steel core-former plates having 80 flow holes per plate that are 1-5/16 in. in diameter and are aligned top to bottom. To characterize melt debris migration behavior within the core-former region, an assessment was made of the potential for

lateral melt migration along the surface of the former plates versus drainage through the flow holes. A comparison of the flow area associated with the breached east-quadrant baffle plate and the flow hole area associated with the fifth-level core-former plate, indicate that the breached baffle plates offer a larger hole area than the former plates. The implication of such a comparison is that lateral migration of molten corium along the surface of the core former plate can be expected. Lateral melt migration is supported by observation of debris found on both the north and east quadrants of the core former plates.

An estimate was also made of a characteristic drainage time for downward melt migration through the core-former holes. Assuming melt debris occupies the entire volume between two stacked former plates, and that all holes in a former plate are available for drainage, a drainage time of approximately 15 s was estimated. The implication of this result is that rapid drainage of melt debris through the former plates would have occurred, <u>if</u> such debris remained molten. However, the fact that a significant amount of debris has been observed to remain in the core-former volume space, and that the reactor vessel is estimated to have been reflooded by ECC injection after 200 min, implies resolidification of once-molten debris in the core-former region upon contact with coolant. In-place refreezing of debris, when exposed to coolant in the core-former volume space, is consistent with the observation of the presence of debris on the former plates.

An examination of debris characteristics (composition, size, surface morphology) and the extent of thermal interaction with the former plates (fused debris to former plate versus loose rubble) is recommended to reveal the nature of melt-debris/former-plate interaction, as well as the debris quenching process. A comparison of melt debris characteristics in the core former region with that in the lower plenum is also recommended, to determine if significant differences in debris composition, mean particle size, and retained fission products exist. These data will enhance understanding of the debris cooling and potential thermal damage to the vessel structural components.

7.3 Lower Head

Thermal damage potential to the lower head was also assessed for the configuration of coherent jet impingement of relocating melt debris. For this assumed configuration, the thermal response of the lower head is largely dictated by the contact time and heat transfer characteristics at the jet impingement surface. Assuming a jet diameter equal to the flow area within a single undegraded fuel assembly, the time for melt relocation as a jet is estimated to be about 75 s. This estimate is consistent with source-range monitor data, indicating that major core relocation occurred over a 1-min period.

Two limiting conditions were assessed with respect to jet-impingement heat-transfer characteristics. The first was for a weak jet, with conduction-limited heat transfer. The second was for strong jet forces, where turbulent mixing and mass transfer effects at the inpact surface lead to an enhanced convective-controlled heat transfer process. For conduction-controlled heat transfer, surface ablation of the lower head by direct impingement is not inferred. This is due to the rather poor conductivity of the molten ceramic material and the high thermal capacity of the vessel head, which serves as an efficient and quick-response heat sink. However, calculational results for convection-controlled heat transfer indicate limited melt ablation at the liner surface. The calculated depth of penetration of the melt front is on the order of about 0.5 in. (versus a head thickness of 5.5 in.) for a jet impingement time on the order of 75 s. A direct jet impingement time of about 15-20 min is, however, calculated to be necessary for melt ablation of the vessel head 1/2-thickness. It is, therefore, concluded that for a jet impingement time of 1 to 2 min (time associated with melt drainage to the lower plenum), little thermal damage to the lower vessel head would result.

An examination of the vessel liner, particularly in the east-quadrant, is recommended to establish whether or not a jet actually channeled its way to the vessel bottom and thermally attacked the lower head. However, because little damage to the lower head is predicted (either for a strong jet or for coherent spreading of melt debris along the head surface), it

may be more useful to examine for melt ablation of the bottom-entry instrument guide tubes and penetration nozzles, since the limited thermal capacity of these structures make them more susceptible to evidence of melt ablation.

In summation, analyses presented in this report indicate that differences in melt-debris induced damage characteristics to the baffle walls, core-former plates, and lower head, are attributed largely to differences in contact time with molten corium, the heat capacity of the various structures, and exposure to coolant. Vessel and debris examination can confirm (or refute) present understanding of melt-debris/structural interactions during the melt progression phase of the TMI-2 accident.

8. REFERENCES

1. V. F. Fricke, Reactor Lower Head Video Inspection, TMI-2 Technical Planning Bulletin, TPB-85-6, February 26, 1985.

2. V. F. Fricke, Reactor Lower Head Video Inspection, TMI-2 Technical Bulletin, TB-85-23 Rev. 0, August 8, 1985.

3. V. R. Fricke, "Fiberscope Inspection Inside CSA," TMI-2 Technical Bulletin, TB-87-4, March 4, 1987.

4. C. M. Allison to J. M. Broughton, "Estimate of TMI-2 Core Damage at 174 Minutes," CMA-11-85, EGG Idaho, Inc., August 15, 1985.

5. J. M. Broughton, "Best-Estimate TMI Core Conditions and Accident Scenario," Proc. of the First International Information Meeting on the TMI-2 Accident, CONF-8510166, Germantown, MD, October 21, 1985.

6. P. Kuan, TMI-2 Core Debris Bed Coolability, EGG-TMI-7150, March 1986.

7. P. Kuan, Core Relocation in the TMI-2 Accident, EGG-TMI-7402, November 1986.

8. E. L. Tolman et al., TMI-2 Accident Scenario Update, EGG-TMI-7484, December 1986.

9. R. Hentry et al., "Core Relocation Phenomenology, Proceedings of the First International Information Meeting on the TMI-2 Accident, CONF-8510166, Germantown, MD, October 1985.

10. V. F. Fricke, "Reactor Lower Head Video Inspection," TMI-2 Technical Bulletin, TB-85-6 Rev. 0 and Rev. 1, February 26, 1985 and March 7, 1985.

11. V. F. Fricke, "Reactor Lower Head Video Inspection - Phase II," TMI-2 Technical Bulletin, TB-86-3 Rev. 0, January 8, 1986.

12. V. R. Fricke, "Hydraulic Disturbance of the Debris in the Bottom Head of the TMI-2 Head," TMI-2 Technical Bulletin, TB-85-20, July 26, 1985.

13. G. Worku, "Core Debris Sample Retrieval from the Lower Head Region," TMI-2 Technical Bulletin, TB-85-21, July 29, 1985.

14. V. F. Fricke, "Description of Standing Fuel Assemblies," TMI-2 Technical Bulletin, TB-87-4, February 23, 1987.

15. A. W. Cronenberg, S. R. Behling, and J. M. Broughton, "Assessment of Damage Potential to the TMI-2 Lower Head Due to Thermal Attack by Core Debris," EGG-TMI-7222, June 1986.

16. S. Bokharee, "Fuel Debris in Region Between Core Former Baffle Plates and Core Barrel," TMI-2 Technical Bulletin, TB 87-9, May 12, 1987.

17. S. Bokharee, "Fuel Debris in Region Between Core Former Baffle Plates and Core Barrel," TMI-2 Technical Bulletin, TB 87-9, Rev. 1, July 9, 1987.

18. H. S. Carslaw, and J. C. Jaeger, Conduction of Heat in Solids, London: Oxford University Press, 1959.

19. W. M. Rohsenow and J. P. Hartnett, Handbook of Heat Transfer, New York: McGraw-Hill Book, Co., 1973, pp. 3-37 to 3-42.

20. J. C. Muehlbauer, and J. E. Sunderland, "Heat Conduction with Freezing or Melting," Applied Mechanics Review, 8, 12, 1965, pp. 951-959.

21. T. R. Goodman, "The Heat-Balance Integral and Its Application to Problems Involving a Change of Phase," J. Heat Trans., 80, 2, 1958, pp. 335-342.

22. M. S. El-Genk and A. W. Cronenberg, "Some Improvements to the Solution of Stefan-Like Problems," Intr. J. Heat Mass Trans. 22, 1979, pp. 167-170.

23. M. S. El-Genk and A. W. Cronenberg, "Stefan-Like Problems in Finite Geometry," Heat Transfer: AICHE Symposium Series No. 189 (75), San Diego 1979, pp. 69-80.

24. A. L. London, and R. A. Seban, "Rate of Ice Formation," Trans. ASME, October 1943, pp. 771.

25. S. Bokharee, GPU Nuclear, private communication, July 22, 1987.

26. D. W. Golden, TMI-2 Standard Problem Package, EGG-TMI-7382, September 1986.

27. V. R. Fricke, "Reactor Lower Head Video Inspection," TMI-2 Technical Planning Bulletin, TPB-85-6, February 26, 1985.

28. IDCOR Report, Debris Coolability, Vessel Penetration, and Debris Dispersal, IDCOR Report-15.1, 1983.

29. A. I. Leont'ev, "Heat and Mass Transfer in Turbulent Boundary Layers," Advances in Heat Transfer 3, 1977, pp. 40-97.

APPENDIX A

DESCRIPTION OF THE CORE FORMER ASSEMBLY

APPENDIX A
DESCRIPTION OF THE CORE FORMER ASSEMBLY

Figure A-1 presents a quarter-section view of the TMI-2 core-former assembly, which comprises the vertical baffle plates at the core periphery and the attached horizontal core-former plates. Also shown are the adjacent core barrel and thermal shield. A summary description of the dimensional characteristics are presented here, based on information given in Reference A-1.

Former Plates

The uppermost horizontal core-former plate is positioned about 10-1/8 in. below the top of the core barrel and 5-7/8 in. below the top of the baffle plate. The bottom former plate is core-positioned 5-7/8 in. above the bottom of the baffle plate. There are 6 intermediate core-former plates, where plate spacing varies from 18 to 25 in.. The former plates have 20 flow holes per core quadrant (80 holes per plate). All flow holes are aligned top to bottom and are 1-5/16-in. diameter, except at the mid-level (fifth) former plate. At this level, four of the flow holes per quadrant are 1-5/16 in. in diameter; the rest are 1 in. diameter. The fifth former plate level, therefore, fixes the minimum open flow area of the core-former plates.

Baffle Plates

The vertical baffle plates shrouding the core periphery are 160-in. high. The baffle plates also have as-fabricated holes which are 1-3/8 in. om diameter. A typical row of holes is located 1-5/8 in. below a corresponding row of bolts that attach the baffle plates to the former plates. The hole spacing in a given row varies from 5 to 9 in. There are no holes adjacent to the upper row nor the two lower rows of attachment bolts. Rows 2, 3, and 6 (from the top) have 80 holes per row. Rows 4 and 5 have 32 holes per row. There is also a 42-3/4-in.-long by

Blank

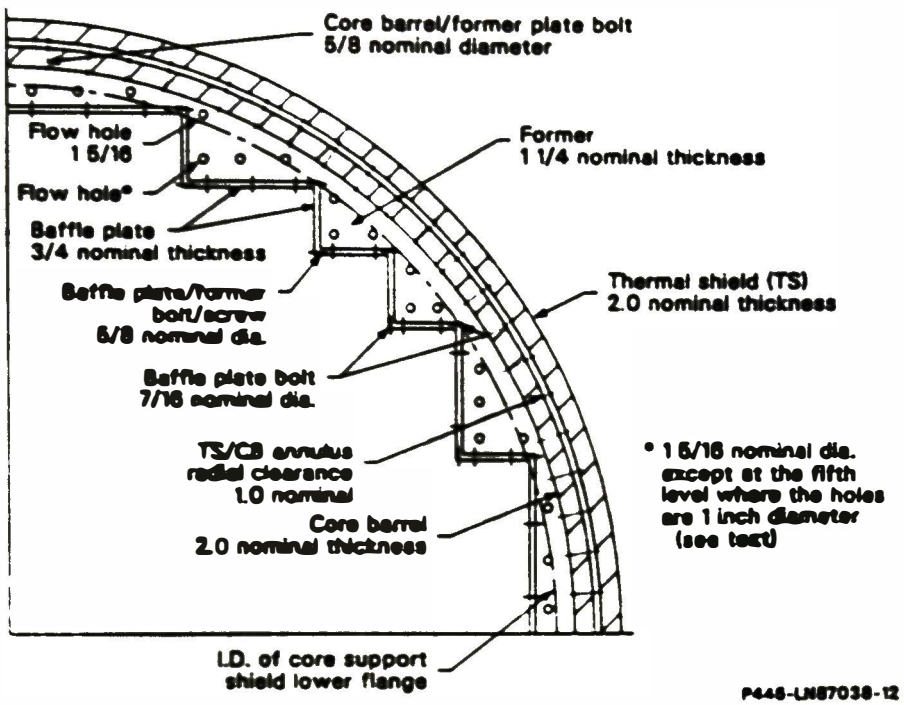

Figure A-1. Illustration of the TMI-2 core-former assembly.

1/4-in.-wide slot on all baffle-plate corners adjacent to the core. These slots are located at about mid-core height. Figure 3-4 illustrates the location of the as-fabricated holes in the baffle plates.

Fastening Characteristics

The core former plates and baffle plates are bolted to each other to form a ridged structure. The 3/4-in.-thick baffle plates are bolted to each other at their edges by 7/16-in.-diameter bolts (612 total). The baffle plates are held to the former plates by 5/8-in.-diameter hex-head bolts and shoulder screws (864 total). The 1-1/4-in.-thick former plates are held to the core barrel by 5/8-in.-diameter cap screws (704 total). All of the above bolts and screws are secured by welded locking pins or rings.

Reference

A-1. S. Bokharee, "Fuel Debris in Region Between Core Former Baffle Plates and Core Barrel," TMI-2 Technical Bulletin, TB 87-9, May 12, 1987.